

IRTF observations of white dwarfs with possible near-infrared excess

J. Farihi^{1,2}

¹*Department of Physics & Astronomy, University of Leicester, Leicester LE1 7RH, UK; jf123@star.le.ac.uk*

²*Visiting Astronomer at the NASA Infrared Telescope Facility*

ABSTRACT

Near-infrared photometry and spectroscopy is obtained for a heterogeneous sample of nearby white dwarfs with possible excess flux as identified primarily in the Two Micron All Sky Survey. Among the sample of 43 stars are a number of white dwarfs that are either metal-rich, magnetic, or binary suspects. With a few notable exceptions in four (or possibly five) distinct categories, the newly obtained *JHK* photometric data fail to corroborate the putative excesses, with $\langle K_{\text{IRTF}} - K_{2\text{MASS}} \rangle = +0.31$ mag. Where available, *GALEX* photometric data are used to better constrain the overall spectral energy distribution of the white dwarfs, enabling any excess near-infrared flux to stand out more readily against the expected stellar photosphere.

With superior data, a near-infrared photometric excess is confirmed at three metal-rich white dwarfs and ruled out at nine others. Several new binaries are confirmed or suggested; five white dwarf - red dwarf pairs and five double degenerates. Four apparently single magnetic white dwarfs – two DA and two DQp – display modest to strong near-infrared excess (relative to non-magnetic models), which may be better described as two effective temperatures owing to a redistribution of energy in highly magnetic or peculiar atmospheres.

Key words: binaries: general — circumstellar matter— infrared: stars— stars: evolution— stars: low-mass, brown dwarfs — white dwarfs

1 INTRODUCTION

The physical parameters of white dwarfs make them excellent targets for binary and multiple system studies. These faint stellar embers permit a relatively unobstructed view, across multiple wavelengths, of their most common companions, low mass main-sequence stars (Farihi et al. 2005). Their Earth-sized radii offer the ultimate, natural, low contrast background for the near-infrared detection of all types of intrinsically faint companions: cool white dwarfs (Zuckerman et al. 1997), ultracool main-sequence dwarfs (Probst 1983), brown dwarfs (Becklin & Zuckerman 1988), and planets (Burleigh et al. 2008). Furthermore, their typical warm to hot stellar effective temperatures give white dwarfs a distinct ultraviolet signature, often detectable against early-type main-sequence companions (Burleigh & Barstow 1998).

White dwarfs come with a hard lower limit on their total age, an attribute lacking in any given non-degenerate field star. Together with an accurate mass estimate, the most likely total age of a white dwarf can be inferred from its most likely progenitor mass and lifetime (Williams et al. 2009; Kalirai et al. 2008; Dobbie et al. 2006). In this way, white dwarfs with substellar companions offer the most accessible,

and best empirical tests of brown dwarf and planetary cooling models at intermediate to older ages (Steele et al. 2009; Burleigh et al. 2009; Farihi et al. 2008a).

In recent years, the advantageous, compact nature of white dwarfs has been extended via the discovery of dust within the Roche radius of more than one dozen stars (Farihi et al. 2009; von Hippel et al. 2007; Jura et al. 2007), the likely result of tidally-disrupted minor bodies perturbed into close approach. This orbital phase space is essentially covered by the diameter of main-sequence stars, where a similar encounter would instead produce an impact. While near-infrared excess emission is measured for about half the white dwarfs with circumstellar dust (Farihi et al. 2009; Kilic et al. 2006), such warm dust is virtually unheard of at their main-sequence progenitors (Zuckerman et al. 2008).

This paper presents the results of an extensive photometric search for near-infrared excess due to low mass stellar and substellar companions, cool white dwarf companions, and warm circumstellar dust. Excess emission is confirmed at a few to several stars in each of these categories, as well as in another group that may be associated with magnetism, peculiar atmospheric composition, or both. The observations and data are presented in §2 and §3, with detailed results

Table 1. SpeX Target Stars

WD	Name	Spectral Type	T_{eff}^a (K)	Data Type	Reference
0023-109	G158-78	DA+DC+dM	10400	Phot	1,2
0106-328	HE	DAZ	15700	Phot	3
0108+277	NLTT 3915	DA	5300	Phot	4,5
0146+187	GD 16	DAZB	11500	Phot	6
0155+069	GD 20	DA	20600	Phot	7
0156+155	PG	DC	9800	Phot	8
0235+064	PG	DAZ+dM	13500	Phot	9,10
0253+508	KPD	DAP	20000	Phot	11
0257-005	KUV	DAO+dM	80900	Phot	1
0408-041	GD 56	DAZ	14400	Phot	3
0518+333	EG 43	DA+dM	9500	Phot	1,12
0939+071	PG	UV+dF	...	Spec	1
0956+045	PG	DA	18200	Phot	13
1000+220	TON 1145	UV+dF	...	Phot/Spec	14
1013-010	G53-38	DA+DC	8800	Phot/Spec	15,16
1036-204	LHS 2293	DQp	7500	Phot/Spec	17
1108+325	TON 60	DA+dM	63000	Phot	13
1133+489	PG	DO+dM	47500	Phot	18
1140+004	SDSS	DA+dM	14400	Phot	19,20
1156+132	LP 494-12	DQp	...	Phot	1
1225-079	PG	DZA	10500	Phot/Spec	21
1254+345	HS	DAH	15000	Phot/Spec	22
1330+015	G62-46	DAH+DC	6000	Phot	23
1339+346	PG	DA	16000	Phot	13
1350-090	LP 907-37	DAP	9500	Phot/Spec	13
1428+373	PG	DA+DC	14000	Phot/Spec	13
1434+289	TON 210	DA	33000	Phot/Spec	13
1455+298	G166-58	DAZ	7400	Phot/Spec	12,13
1457-086	PG	DAZ	20400	Phot	3
1619+525	PG	DA+dM+dM	18000	Phot	13
1626+368	G180-57	DZA	8400	Spec	24
1653+385	NLTT 43806	DAZ	5700	Phot	4
1845+683	KUV	DA	36000	Phot	25
2032+188	GD 231	DA+DC	18500	Phot	26,27
2144-079	G26-31	DBZ	16500	Phot	28
2201-228	HE	DB	18000	Phot	29
2211+372	LHS 3779	DC	6000	Phot	30
2215+388	GD 401	DZ	8800	Phot	31
2216+484	GD 402	DA+DC	7000	Phot	32
2316+123	KUV	DAP	10400	Phot	11
2333-049	G157-82	DA	10500	Phot	33
2336-187	G273-97	DA	8100	Phot	33
2354+159	PG	DBZ	24400	Phot	28

^a The effective temperatures in the fourth column are previously published values unless otherwise stated; these values do not always agree with the fits shown in the figures.

References: 1) This work; 2) Catalán et al. 2008; 3) Koester et al. 2005a; 4) Kawka & Vennes 2006; 5) Farihi et al. 2009; 6) Koester et al. 2005b; 7) Homeier et al. 1998; 8) Putney 1997; 9) Zuckerman et al. 2003; 10) Farihi et al. 2008b; 11) Liebert et al. 1985; 12) Bergeron et al. 2001; 13) Liebert et al. 2005a; 14) Green et al. 1986; 15) Pauli et al. 2006; 16) Nelemans et al. 2005; 17) Liebert et al. 2003; 18) Dreizler & Werner 1996; 19) Kleinman et al. 2004; 20) Vennes et al. 2002; 21) Wolff et al. 2002; 22) Hagen et al. 1987; 23) Bergeron et al. 1993; 24) Dufour et al. 2007; 25) Napiwotzki et al. 1999; 26) Bergeron et al. 1992; 27) Morales-Rueda et al. 2005; 28) Voss et al. 2007; 29) Jordan 2001; 30) Greenstein & Liebert 1990; 31) Dupuis et al. 1993; 32) Bergeron et al. 1990; 33) Koester et al. 2001

on individual objects given in §4, and a brief discussion in §5.

2 OBSERVATIONS & DATA

The majority of the 43 targets listed in Table 1 come from the white dwarf catalog of McCook & Sion (1999), and were selected because their Two Micron All Sky Survey (2MASS) JHK_s photometry suggested near-infrared excess emission. These are primarily white dwarf plus low mass stellar or substellar companion candidates, a significant fraction of which are taken from Farihi et al. (2005), and Wachter et al. (2003). A small number of these stars are known or suspected magnetic white dwarfs, but were not intentionally selected as such, and hence these targets overlap with the sample analyzed by Wellhouse et al. (2005). Another subset of targets were chosen from various literature sources as binary suspects based on optical spectroscopy and photometry; many of these are double degenerate suspects (e.g. Bergeron et al. 1990). A final subset of targets are metal-rich white dwarfs with low or questionable quality 2MASS photometry, most of which are part of various *Spitzer* programs aimed at searching for circumstellar dust (Farihi et al. 2009, 2008b; Jura et al. 2007).

Data were obtained at the NASA Infrared Telescope Facility (IRTF) using the medium-resolution spectrograph and imager SpeX (Rayner et al. 2003) on 2006 October 7–9 and 2007 April 7–9. Conditions were photometric or near-photometric for all of the imaging observations, while thin cirrus was present during some of the spectroscopy. The instrument was used primarily for imaging, but also in its intended spectrographic configuration. Science target images were taken at JHK using individual exposure times that were typically 30 seconds. A seven point dither pattern was repeated once or twice, resulting in total integration times between 3.5 and 7.0 minutes. Photometric standard stars were observed in a similar manner a few to several times during each night to measure the zero point in each pass-band.

Spectroscopy of select targets was performed with SpeX using the low-resolution prism mode that covers the entire $0.8 - 2.5 \mu\text{m}$ region in a single exposure setting. The $0''.8$ slit was used to maximize gathered light at the expense of resolution, resulting in $R \approx 100$ at H band. Individual exposures of 120 seconds were used at two positions along the slit, repeated ten times for a total integration time of 20 minutes. An A0V telluric standard star was observed immediately following each science observation, as were spectral flat fields and arc lamp images.

Near-infrared images for 41 targets were reduced in the standard fashion, with long exposure sky frames normalized to serve as flat fields. Images of each target at each band-pass were sky-subtracted by removing the median of the raw image stack, flat-fielded, then registered and recombined by averaging. Photometry of science targets and standard stars was performed with aperture radii between $r = 10$ and 20 pixels, corresponding to $1''.5 - 3''.0$, and generally measured at the widest possible radius while avoiding contamination from nearby objects or companions. Where possible, 2MASS sources within the SpeX field of view were used to corroborate the photometric calibration. Median extinction values

for Mauna Kea were used to correct all photometry to air-mass 1.00, and the zero point of each filter for each night was established by averaging the measurements for three to four standard stars. The zero points for all nights during both observing runs were found to agree within a few percent.

Spectroscopic data for 11 targets were reduced with Spextool (Cushing et al. 2004), including sky-subtraction, flat-fielding, spectral extraction and averaging. Spextool also was used to perform wavelength calibration, telluric feature removal, sensitivity correction, and flux calibration. However, due to slit losses and other sources of error, the final flux calibrations of the science target spectra were established using photometry.

3 ANALYSIS

The resulting near-infrared photometry and spectroscopy for all 43 targets are listed in Table 2 and plotted together with the ultraviolet and optical spectral energy distributions in Figures A1 – A52, ordered by right ascension. Optical photometric data plotted in the figures were taken from various literature sources, including but not limited to the Sloan Digital Sky Survey (Adelman-McCarthy et al. 2008), DENIS (DENIS Consortium 2005), the white dwarf catalog of McCook & Sion (1999) and references therein. There are a few cases with photographic photometry (Space Telescope Science Institute 2006; Copenhagen University Observatory 2006; Zacharias et al. 2005; Monet et al. 2003) where superior data were unavailable. The SDSS fluxes were assumed to have 5% errors for the following reasons: 1) the quoted photometric errors in SDSS DR7 are often less than 0.01 mag, which is unlikely to be realistic; 2) where two flux measurements of a single source are available, they sometimes differ by 5% or greater in a given bandpass; 3) many of the flux measurements carry middle-grade photometric quality flags; and 4) several objects cataloged as point sources are in fact members of close double or multiple systems, implying further photometric error. Additionally, available *GALEX* far- and near-ultraviolet fluxes are included in the plots; a weighted average was taken where multiple measurements are given. These fluxes are uncorrected for extinction, and minimum 10% errors have been assigned. Where available, 2MASS JHK_s photometry (Skrutskie et al. 2006) is plotted alongside the IRTF data for direct comparison.

The optical and ultraviolet photometry for all stars were fitted with model spectra of the appropriate effective temperatures, which sometimes deviated from previously published literature values. Hydrogen atmosphere stars were fitted with $\log g = 8.0$ white dwarf spectral models of Koester (2009), while blackbody spectra were used for helium-rich stars. In most cases, the model T_{eff} could be adjusted to match the near-infrared photometry, consistent with emission from the stellar photosphere. In cases where a potential near-infrared excess was indicated in a single or multiple bandpasses, those data were not employed to adjust the model fits. The white dwarf mass (via $\log g$) was not varied in the model fits, as the focus of the study was to establish the presence or absence of a near-infrared excess, which is best achieved by constraining the stellar T_{eff} . While white dwarf colors are, to second order, affected by $\log g$,

errors resulting from fixing $\log g$ in the model fits should be of the same order or smaller than the uncertainty in T_{eff} itself (Bergeron et al. 1995b). Where utilized for distance estimates to binary and multiple system components (Table 3), white dwarf model parameters (masses, radii, colors, and absolute magnitudes) were taken from Bergeron et al. (1995a,b), while empirical low mass stellar parameters were evaluated using the colors and absolute magnitudes given in Kirkpatrick & McCarthy (1994).

4 RESULTS FOR INDIVIDUAL OBJECTS

0023–109 . G158-78 is a likely triple system. Eggen & Greenstein (1965) first reported a co-moving, cool companion, G158-77, henceforth designated G158-78B. The wide pair are separated by $59''.4$ at position angle 330° based on analysis of archival plates dating from 1954.7, 1983.6 and 1998.8. Modern astrometry yields a proper motion of $(72, -205)$ mas yr $^{-1}$ for the white dwarf (Salim & Gould 2003), and $(74, -206)$ mas yr $^{-1}$ for the secondary (Zacharias et al. 2004). G158-78B has $V - K = 3.5$ (Reid 1996), indicating a spectral type of M0V at a photometric distance of 92 pc (Kirkpatrick & McCarthy 1994).

Reid (1996) reported radial velocity variations in the white dwarf G158-78A, with at least one value clearly incompatible with the radial velocity of G158-78B. While the broad-band optical colors of the primary suggest a 7000 K star, high quality spectroscopic data reveal an effective temperature near 10000 K (Catalán et al. 2008; Kleinman et al. 2004). This higher temperature, necessary to explain the *GALEX* data for this white dwarf, implies the red optical and near-infrared fluxes are greater than expected for a single star. Figure A1 shows the complete spectral energy distribution is well reproduced by the addition of a low-luminosity companion with temperature around 6500 K. The implied tertiary star, G158-78C, can only be another white dwarf.

0106–328 . The coordinates of this warm DAZ star are inaccurate in SIMBAD, but correct to within several arcseconds in the current online version of McCook & Sion (2008). Its 2MASS position is $01^{\text{h}}08^{\text{m}}36.03^{\text{s}} -32^\circ37'43''.6$ (J2000). There is no photometric nor spectroscopic *K*-band excess at this polluted white dwarf (Kilic et al. 2008).

0108+277 . NLTT 3915 is located a few arcseconds away from a background star (Farihi et al. 2009) that is perhaps responsible (by contaminating sky apertures) for the lower fluxes reported in 2MASS versus the IRTF values.

0146+187 . GD 16 has a mid-infrared excess from warm circumstellar dust (Farihi et al. 2009). The IRTF photometry disagrees somewhat with 2MASS at *J* band, but is consistent with the white dwarf effective temperature (Koester et al. 2005b). The *GALEX* detection of GD 16 appears on the edge of the array, and is unlikely to be reliable.

0155+069, **0156+155**, **1434+289**, **2144–079**, **ε 2211+372** . The apparent 2MASS excesses at these stars are spurious.

0235+064 . This PG star is located several arcseconds from a common-proper motion companion M dwarf. The companion has likely caused some prior studies of the white dwarf to underestimate its effective temperature via contamination of optical data (Farihi et al. 2008b). All data presented here is unaffected by the light of the dM companion, and a model fit to the full spectral energy distribution yields $T_{\text{eff}} \approx 13500$ K. Assuming $\log g = 8.0$ places the system at 62 pc, consistent with a companion spectral type of M3.5 ($V - K = 4.9$) at that distance.

0253+508 . The ultraviolet and optical data for this star are well-modeled with a $T_{\text{eff}} = 20000$ K hydrogen atmosphere, non-magnetic white dwarf (Liebert et al. 1985; Downes & Margon 1983), as can be seen in Figure A8. However, the $V - K = -0.16$ color is suggestive of a much cooler star, near 10000 K. Whether the *JHK* excess (relative to non-magnetic models) emission is photospheric in nature remains to be seen, but the fluxes are not consistent with a low mass star or brown dwarf (Farihi et al. 2005), nor circumstellar dust (Kilic et al. 2006). It is possible that the highly magnetic stellar atmosphere is causing an emergent two-temperature appearance and further investigation is warranted.

0257–005 . This system is resolved into two components separated by $1''.0$ in *HST* / ACS observations (Farihi et al. 2009, in preparation). The binary is also partially resolved in the IRTF observations, but only photometry for the composite double was possible. Near-infrared data alone does not strongly constrain the companion parameters, but the ACS data yield $I - K = 2.6$ and an estimated spectral type of M4.5 at 490 pc.

Eisenstein et al. (2006) list the primary star as type sdO with $T_{\text{eff}} = 69000$ K and $\log g = 5.9$, yet only white dwarfs should attain such high temperatures. These parameters may be due to a problematic automated fit to the SDSS spectrum and photometry; a mild red continuum and a few late-type stellar features are present in the data beyond 6000 Å. Visual examination of the spectrum indicates a likely DAO white dwarf, a hypothesis corroborated by the implied distance to the M dwarf companion; at 490 pc, the primary would be intrinsically too faint for a horizontal branch star (Lisker et al. 2005).

Following the method of Rebassa-Mansergas et al. (2007), a fit to the SDSS spectrum yields $T_{\text{eff}} = 80900 \pm 7600$ K and $\log g = 7.13 \pm 0.34$, verifying KUV 0257–005 is a DAO white dwarf. Allowing for some mild extinction in the optical yields a photometric distance of 1040 ± 330 pc, which can only be matched by the cool companion if it is an equal luminosity double at 700 pc. Further observations are required to test this scenario.

0408–041 . GD 56 has a rare, strong infrared excess due to circumstellar dust that manifests beginning at *H* band (Kilic et al. 2006). The IRTF photometry corroborates this finding, and improves significantly upon 2MASS data.

0518+333 . EG 43 (G86-B1B, NLTT 14920) is part of a common-proper motion binary with an M dwarf (G86-B1A, NLTT 14919; Salim & Gould 2003) $7''.4$ distant. The white

Table 2. Near-Infrared Photometry

WD	$J_{2\text{MASS}}$ (mag)	$H_{2\text{MASS}}$ (mag)	$K_{2\text{MASS}}$ (mag)	J_{IRTF} (mag)	H_{IRTF} (mag)	K_{IRTF} (mag)	Excess Type ^a
0023–109	16.05(08)	15.84(17)	15.68(25)	15.97	15.85	15.93	1
0106–328	15.75(08)	15.78(17)	...	15.75	15.78	15.92	...
0108+277	15.22(06)	15.04(08)	14.87(13)	15.03	14.79	14.72	...
0146+187	15.80(08)	15.53(10)	15.36(16)	15.55	15.51	15.29	2
0155+069	15.81(08)	15.47(13)	...	15.75	15.78	15.96	...
0156+155	15.74(08)	15.44(11)	...	15.60	15.56	15.57	...
0235+064	15.69(07)	15.91(20)	...	15.73	15.77	15.87	...
0253+508	15.58(06)	15.31(11)	15.07(12)	15.44	15.36	15.38	3
0257–005	16.77(14)	16.34(21)	15.53(20)	16.52	16.18	15.96	4
0408–041	15.87(06)	15.99(13)	15.44(18)	15.85	15.75	15.13	2
0518+333	15.37(09)	15.12(21)	14.81(16)	15.91	15.87	15.89	1
0939+071	13.99(03)	13.68(04)	13.60(03)
0956+045A	16.41	16.38	16.45	...
0956+045B ^b	14.66(04)	14.13(05)	13.84(06)	14.67	14.21	13.85	...
1000+220	16.28(10)	15.97(21)	15.67(23)	16.21	16.21	16.33	...
1013–010	14.79(03)	14.61(06)	14.71(12)	14.80	14.65	14.64	1
1036–204	14.63(03)	14.35(04)	14.04(07)	14.62	14.31	14.09	5
1108+325	15.80(07)	15.19(08)	15.23(18)	15.77	15.29	15.13	4
1133+489	16.19(09)	15.68(14)	15.41(16)	16.16	15.75	15.55	4
1140+004	15.55(07)	15.06(08)	15.12(16)	15.60	15.12	14.83	4
1156+132	16.95(15)	17.32	17.38	17.08	5
1225–079	14.88(04)	14.92(08)	14.85(12)	14.78	14.80	14.80	...
1254+345	16.70(13)	16.14(19)	...	16.58	16.50	16.56	...
1330+015	16.40(12)	16.30(21)	...	16.31	16.27	16.24	1
1339+346	14.09(03)	13.70(03)	13.59(03)	16.06	16.07	16.15	...
1350–090	...	14.15(05)	...	14.23	14.12	14.12	...
1428+373	15.80(06)	15.57(09)	15.58(23)	15.54	15.61	15.74	...
1434+289	16.51(12)	16.33(20)	15.92(29)	16.43	16.52	16.70	...
1455+298	14.97(05)	14.61(08)	14.74(13)	14.85	14.74	14.72	...
1457–086	16.04(10)	16.21(23)	15.62(23)	16.08	16.10	16.03	2
1619+525AB	15.34	15.10	14.95	4
1619+525C ^b	14.17(03)	13.55(04)	13.43(04)	14.18	13.60	13.39	...
1626+368	13.64(02)	13.65(03)	13.58(04)
1653+385	15.53(06)	15.35(11)	15.27(15)	15.62	15.36	15.25	...
1845+683	16.07(09)	16.28(22)	...	15.98	16.24	16.30	...
2032+188	15.80(10)	15.53(17)	15.26(23)	15.68	15.71	15.73	...
2144–079	15.03(05)	15.21(10)	14.90(14)	15.14	15.21	15.31	...
2201–228	16.28(10)	15.97(21)	15.67(23)	16.21	16.21	16.33	...
2211+372	16.25(10)	16.06(19)	15.62(24)	16.12	16.05	15.89	...
2215+388	16.14(10)	16.02	16.01	16.03	...
2216+484	15.48(06)	15.30(10)	15.32(16)	15.36	15.25	15.18	1
2316+123	15.47(06)	15.72(15)	15.14(19)	15.49	15.51	15.56	3
2333–049	15.73(05)	15.72(11)	15.48(19)	15.71	15.74	15.66	...
2336–187	15.06(04)	14.94(06)	14.68(09)	15.04	14.92	14.89	...
2354+159	16.22(12)	16.02(17)	15.52(24)	16.19	16.21	16.27	...

Photometric errors for the IRTF data are 5%.

^a The near-infrared excesses listed in the final column are associated with: 1) a cool white dwarf companion; 2) warm circumstellar dust; 3) a magnetic DA, relative to non-magnetic models; 4) a red dwarf companion; 5) a magnetic DQ, relative to non-magnetic models.

^b Not a white dwarf, but a spatially resolved red dwarf companion

dwarf itself is a double degenerate suspect, but that assessment was based on $T_{\text{eff}} \approx 7800$ K (Bergeron et al. 2001), and almost certainly a result of *VRIJHK* photometry contaminated by the M dwarf companion. This is a good possibility, as the M dwarf outshines the white dwarf at *B* and *V* bands by around 0.4 and 1.8 magnitudes, respectively (Reid 1996; Massey et al. 1995). Furthermore, the IRTF data differ quite

significantly from the near-infrared data of Bergeron et al. (2001), as can be seen in Figure A11.

Using the *UBV* photometry from Massey et al. (1995), a 9500 K DA white dwarf model appears to reproduce the *UBVJHK* data rather well. At the parallax distance of 65.4 pc ($\pi = 15.3 \pm 2.2$ mas; van Alena et al. 1995), the white dwarf should have $M_V = 12.0 \pm 0.3$ mag, a range that

includes $\log g = 8.0$ at this higher effective temperature. Therefore, the white dwarf should no longer be considered a double degenerate suspect.

The M dwarf companion has $V - K = 4.5$, consistent with a spectral type of M3. However, the implied $M_K = 5.7$ mag at 65.4 pc is brighter than expected for this spectral type. Indeed, this star is a visual binary separated by $0''.2$ with *HST* / ACS, making the system a triple (Farihi et al. 2009, in preparation). Assuming equal luminosity gives each star in G86-B1AC $M_K = 6.5$ mag, consistent with M3 spectral types implied by their color.

0939+071 . This star has persisted among white dwarf lists over the years lacking any high quality observations in the literature. Its status as a degenerate star rests firstly with Greenstein (1984), who lists it as a weak-lined DA of temperature near 7200 K, and secondly upon Green et al. (1986), who list the star as DC in the same temperature class, with a blue photoelectric color index of $U - B = -0.55$. However, the $V = 14.9$ mag star has a very small proper motion on the order of 10 mas yr^{-1} (Adelman-McCarthy et al. 2008; Farihi et al. 2005), and its optical spectrum reveals calcium H and K lines (A. Gianninas 2008, private communication; see Figure A12). Together, these data indicate a main-sequence F-type star, with the former more likely based on the strength of the Balmer lines compared to Kurucz models¹

Interestingly, the star has a clear blue-ultraviolet excess at *GALEX* and optical wavelengths that cannot be reproduced by a single temperature component, and is most readily explained by a hot subdwarf or very hot white dwarf companion. However, for this to be the case, the far-ultraviolet flux would have to suffer from a significant degree of extinction. Figures A12 – A14 display various data for this star, which strongly support both an ultraviolet and blue optical excess, relative to a main-sequence F or G-type star. High-resolution observations of this object taken by the SPY survey with VLT / UVES also reveal a clear blue-ultraviolet excess (R. Napiwotzki 2009, private communication).

0956+045 . This PG white dwarf is part of a visual double separated by $2''.0$ (Farihi et al. 2005), and the M dwarf companion dominates the binary light redward of $0.8 \mu\text{m}$. Spatially-resolved *JHK* photometry from the IRTF matches the predictions of an 18000 K DA model (Liebert et al. 2005a). SDSS *griz* photometry of PG 0956+045B provides new color information, and when combined with its near-infrared photometry, indicate an updated spectral type of M5 (Bochanski et al. 2007).

1000+220 . TON 1145 appears similar to PG 0939+071 in a few ways; its data are shown in Figures A16–A18. First, its blue optical spectrum appears to be F-type with similar line strengths. Second, while a main-sequence stellar model fits nearly all the photometric data, there may be an ultraviolet excess, but unfortunately, there are no *GALEX* data for this star. Third, it has a proper motion of order 10 mas yr^{-1} , meaning it is quite distant. A late A-type or early F-type star fits most of the photometric data excepting the SDSS

ug fluxes, perhaps indicating a hot subdwarf or very hot white dwarf companion.

1013–010 . G53-38 is a confirmed double degenerate, a single-lined spectroscopic binary (Nelemans et al. 2005). From Figure A19, there appears to be photometric evidence of the hidden white dwarf companion. Pauli et al. (2006) give 8800 K for the primary based on Balmer line spectroscopy, that underpredicts the red optical and near-infrared fluxes substantially. A combination of a 9000 K DA white dwarf and a $T_{\text{eff}} \sim 6000$ K DC white dwarf is able to reproduce the entire spectral energy distribution quite well.

1036–204 . LHS 2293 is a DQ peculiar white dwarf that displays two clearly disparate effective temperatures, even while excluding the heavily absorbed $4000 - 6000 \text{ \AA}$ region (Jordan & Friedrich 2002; Schmidt et al. 1999). The *GALEX* near-ultraviolet and optical *URI* photometry can be fitted with a 7500 K star, consistent with the analysis of Liebert et al. (1978), while the *IJK* photometry can be reproduced by a 4300 K blackbody. This could be a spectacular example of energy redistribution in a highly unusual atmosphere; clearly more data are warranted for this highly magnetic white dwarf.

1108+325 . This is a visual binary separated by $0''.2$ as imaged with *HST* / ACS (Farihi et al. 2009, in preparation). The improved *JHK* data here indicate $I - K = 2.1$ and a dM3 companion, consistent with the estimated white dwarf distance of 560 pc (Liebert et al. 2005a).

1133+489 . Farihi et al. (2006) resolve this binary at $0''.1$ with *HST* / ACS. The improved *JHK* data here indicate $I - K = 2.7$ for PG 1133+489B, and a dM5 companion, consistent with a 370 pc distance to a $\log g = 8.0$ white dwarf with $T_{\text{eff}} = 47500$ K.

1140+004 . The optical spectrum of this star reveals two strong components, a white dwarf in the blue and an M dwarf in the red. The companion spectral type has been estimated previously to be M4 (Raymond et al. 2003) and M6 (Silvestri et al. 2006). The IRTF near-infrared data permit a broad-band color analysis of the companion that yields $I - K = 2.6$ and an estimated spectral type of M5. This is consistent with the 240 pc distance to a $T_{\text{eff}} = 14500$ K, $\log g = 8.0$ white dwarf (Kleinman et al. 2004).

1156+132 . LP 494-12 is a DQ peculiar star with a relatively warm effective temperature. Ongoing coverage of this region by the UKIRT Infrared Deep Sky Survey (UKIDSS) confirms the IRTF *K*-band excess, reporting $(H, K) = (17.32, 17.08)$ mag for this white dwarf. The nature of the excess emission may be related to its unusual atmosphere or a strong magnetic field (or both), and could be a redistribution of emergent energy as potentially seen in LHS 2293. If correct, the excess at LP 494-12 is still unusual as it only manifests beyond the *H* band.

1225–079 . A strong 8600 \AA calcium absorption feature is clearly detected in this DZA white dwarf. The individual lines of the triplet are unresolved at the resolution of the SpeX prism.

¹ <http://www.stsci.edu/hst/observatory/cdbs/k93models.html>

1254+345 . Using non-magnetic DA models, an effective temperature of 9500 K is estimated for this highly magnetic white dwarf (see Figure A27). This is considerably lower than the previous estimate of 15000 K (Hagen et al. 1987), and is consistent with the slope of its optical, SDSS spectrum.

1330+015 . G62-46 is a likely DAH+DC binary based on spectra that reveal diluted, Zeeman-split lines of $H\alpha$ (Bergeron et al. 1993). Figure A28 essentially reproduces the double degenerate model fit of Bergeron et al. (1993) with 9500 K DC, and 6000 K DA components. However, the I -band flux differs significantly from the SDSS iz photometry, that appear to be corroborated by DENIS I -band data. Using the SDSS and IRTF data, the full spectral energy distribution cannot be modeled within the photometric errors as either a single or double source; the resulting composite either overpredicts the HK , or underpredicts the iz fluxes. The SDSS catalog lists a 'good' quality flag for this photometry, and hence variability may be present. A less likely possibility is near-infrared flux suppression in the cooler DA component. The *GALEX* near-ultraviolet and u -band fluxes may favor a DC component closer to 8000 K.

1339+346 . Part of an apparent stellar triple at galactic latitude $|b| = 77^\circ$, the white dwarf is not physically associated with the remaining pair of stars, currently located $2''.6$ and $21''.2$ distant. This pair of cool stars appear to be co-moving at $(27, -37)$ mas yr $^{-1}$ (Zacharias et al. 2005), while their SDSS and IRTF colors suggest they are main-sequence K stars at roughly 720 pc.

Utilizing an epoch 1950.4 POSS plate scan compared with the epoch 2007.4 IRTF J -band image, the white dwarf has clearly moved relative to the K stars by a few arcseconds. From the motion relative to the nearest K star, a total proper motion of $(80, -72)$ mas yr $^{-1}$ is calculated for the white dwarf.

1350-090 . The DA model fitted to the broad energy distribution in Figure A31 yields an effective temperature around 1000 K lower than the spectroscopically derived value of Liebert et al. (2005a). LP 907-37 is a DAP white dwarf with a kG magnetic field (Schmidt & Smith 1994); the Zeeman split hydrogen lines (Koester et al. 2005a) cannot be seen in the low resolution SpeX prism data. The 2MASS catalog lacks JK_s photometry for this $m < 14.5$ mag white dwarf.

1428+373 . The DA model fitted to the broad energy distribution in Figure A32 yields an effective temperature around 1000 K lower than the spectroscopically derived value of Liebert et al. (2005a).

1455+298 . This is another case where the SDSS iz photometry deviates significantly from the I -band flux of Bergeron et al. (2001). The SpeX prism data appear to agree well with the SDSS fluxes. The apparent 2MASS H -band photometric excess for this white dwarf is spurious.

1457-086 . The apparent 2MASS K_s -band excess at this metal-rich white dwarf is real, but significantly milder in

the IRTF photometry. Optical Balmer line spectroscopy of this star by two independent studies yields $T_{\text{eff}} = 21500$ K (Liebert et al. 2005a) and 20400 K (Koester et al. 2005a), yet such models cannot reproduce the $UBVIJH$ fluxes in Figure A35. A 20000 K DA model fitted to the $UBVI$ photometry predicts the measured J -band flux is in excess of the expected white dwarf photosphere. The optical photometry of Kilkenny et al. (1997) may be somewhat uncertain, but with only these data available, an 18000 K model reproduces all the photometric fluxes excepting K band; consistent with an excess due to warm dust (Farihi et al. 2009).

1619+525 . This is a possible triple system (Farihi et al. 2006) consisting of a white dwarf and a cool main-sequence companion separated by $0''.5$ at position angle 24° , together with another cool companion at $2''.6$ and position angle 283° . The IRTF images spatially resolve PG 1619+525AB from C, and when combined with their *HST* / ACS F814W photometry, imply earlier companion spectral types than previously suspected based on the nominal 100 pc photometric distance to the white dwarf (Farihi et al. 2006; Liebert et al. 2005a).

However, the likely companions both yield consistent photometric distances near 300 pc: PG 1619+525B has $K = 15.3$ mag, $I - K = 2.8$, while PG 1619+525C has $K = 13.4$ mag, $I - K = 1.9$, compatible with spectral types M5 and M2 respectively. Common proper motion has not been established for these stars, yet a physical association is probable based on their proximity and high galactic latitude (Farihi et al. 2006). The probability of a chance alignment with an M dwarf at 300 pc within a cylinder of $r = 0''.5$ and length 100 pc centered on the white dwarf is less than 1 in 5×10^5 , while for two M dwarfs within $r = 2''.6$ the probability is less than 1 in 2×10^6 . The odds would be somewhat greater for distant background stars with reddened I -band magnitudes, yet ultimately unlikely.

Examination of epoch 1954.5 POSS I plates reveals little appreciable motion relative to SDSS images taken in 2004.5; USNO-B1 gives a proper motion for the composite triple of $(34, -12)$ mas yr $^{-1}$, favoring a distant system ($v_{\text{tan}} = 17$ km s $^{-1}$ at 100 pc versus 51 km s $^{-1}$ at 300 pc). Yet the white dwarf parameters derived via Balmer line spectroscopy do not permit such a distant interpretation, as it would imply a temperature inconsistent with the UBV photometry and slope of the optical spectrum, or an extremely low surface gravity. For the time being, the physical association of these three stars remains tentative.

1626+368 . G180-57 is a DZA with a strong 8600 Å calcium absorption feature detected in its spectrum. The individual lines of the triplet are unresolved at the resolution of the SpeX prism. It is unclear why the SDSS photometry differs significantly with available optical fluxes from Bergeron et al. (2001) and several similar measurements (McCook & Sion 1999); variability appears possible in this star.

1653+385 . NLTT 43806 is listed among nearby white dwarfs with a photometric distance of 15 pc (Holberg et al. 2008; Kawka & Vennes 2006), based on an estimated $V = 15.9$ mag (Salim & Gould 2003). The SDSS photometry implies a distance greater than 20 pc, with $g = 17.0$ mag ($V \approx 16.8$ mag) and $d = 24$ pc.

1845+683 . This white dwarf is neither a binary nor binary suspect. Green et al. (2000) incorrectly identified this extreme ultraviolet source with a nearby, unrelated near-infrared source (Farihi et al. 2006).

2032+188 . GD 231 is a double degenerate (Morales-Rueda et al. 2005) and may display mild near-infrared excess due to its unseen companion, but the larger 2MASS excess is not confirmed. Figure A40 demonstrates that the entire spectral energy distribution can be decently matched by a 16500 K DA model, but this may simply reflect a good approximation of the composite light rather than an accurate effective temperature of either component. Assuming the 18500 K spectroscopic temperature derived by Bergeron et al. (1992) is correct, Figure A41 predicts an excess at *JHK* that is consistent with a 6000 K DC companion.

2201–228 . This star was tentatively classified as a magnetic DA, but has since been correctly reclassified as DB (Jordan 2001). The apparent 2MASS excess at this white dwarf is not confirmed; the 13000 K fit to its spectral energy distribution shown in Figure A43 is the first time an effective temperature has been assessed for this DB star.

2215+388 . The *U*-band photometry for this DZ star appears influenced by its strong Ca H and K absorption, and possibly other elements (Sion et al. 1990).

2216+484 . GD 402 is a suspected DA+DC system based on the fact that its optical colors (and the shape of its optical spectrum) predict a significantly higher effective temperature than do its relatively weak Balmer lines (Bergeron et al. 1990). Although the expanded spectral energy distribution – including the IRTF near-infrared data – can be nearly reproduced by a single 7000 K component as shown in Figure A46, the photometry can also be well-modeled with two white dwarf components of approximately 8000 K and 5000 K (Figure A47).

2316+123 . This magnetic white dwarf has a spectral energy distribution that cannot be fitted by a single temperature (non-magnetic) white dwarf model. Figure A48 fits the combined ultraviolet and optical fluxes to yield a temperature near 13000 K, while Figure A49 fits the combined optical and near-infrared colors with a temperature around 10500 K. It is unclear whether this difficulty is related to the magnetic nature of the star, or if there is a real *JHK* photometric excess (relative to non-magnetic models), implying the possibility of binarity.

2333–049 . This white dwarf may have a small *K*-band excess, but more data are needed to confirm or rule out this possibility; the *V*-band flux appears too bright for the model shown in Figure A50.

2336–187 . G273-97 is by far the best near-infrared excess candidate based on its 2MASS data, which appear reliable at all wavelengths. However, the IRTF observations demonstrate that the 2MASS catalog contains significant errors even at $S/N > 10$.

2354+159 . Both Voss et al. (2007) and Beauchamp et al. (1999) give $T_{\text{eff}} \approx 24500$ K – assuming no hydrogen – for this DBZ star. However, both authors give alternative effective temperatures near 22500 K for a nominal hydrogen abundance. The higher temperature overpredicts the *GALEX* fluxes for this star, and the fit shown in Figure A52 employs a temperature of 21500 K to match all the photometry; possibly indicating some hydrogen is present and closer to the 19000 K value given by Koester et al. (2005a).

This white dwarf is another exemplary case of a 2MASS excess not being corroborated by targeted *JHK* photometry; the lack of infrared excess is also confirmed by *Spitzer* IRAC observations (Farihi et al. 2009).

5 DISCUSSION

5.1 Near-Infrared Excesses Predicted by 2MASS

The white dwarf fluxes in the 2MASS catalog were the prime motivation for obtaining follow up data, hence it is relevant to ask how well they predicted the IRTF *JHK* photometry, and the presence of any near-infrared excess. Figure 1 compares the IRTF and 2MASS fluxes (in Vega magnitudes) for all 39 Table 2 white dwarf targets with both sets of photometry; transformations between filter sets were ignored as they are generally within a few percent (Carpenter 2001).

The 2MASS 10σ minimum detection limit for the whole sky is $(J, H, K_s) = (15.8, 15.1, 14.3)$ mag (Skrutskie et al. 2006), and there is decent accord for measurements brighter than this limit. The generally disagreeable behavior of the 2MASS data below the 10σ limit in all three filters is not surprising, yet is most pronounced in the *K* band. Somewhat unexpectedly, the *J*-band shows several discordant measures at the $1 - 2\sigma$ level at relatively bright stars. In fact, of the co-observed white dwarfs at each bandpass, the *H*-band 2MASS data agree most frequently with the IRTF observations over all brightnesses. At the 1σ level, the 2MASS and IRTF photometry agree for 29 of 37 stars (78%) at *H*, 25 of 38 stars (66%) at *J*, and 14 of 29 stars (48%) at *K*.

An infrared excess is revealed by the relative flux levels of three or more photometric fluxes, at least two of which should be consistent with photospheric emission and at least one of which is significantly higher than expected for the photosphere alone. Using this practical definition, the 2MASS photometry suggest an *H* and/or *K_s*-band excess – relative to 2MASS *J* or ultraviolet/optical photometry – for 27 white dwarfs in Table 2. The potential excess fluxes are most readily discerned in the Figures, and where confirmed by the IRTF data, these excesses are often of a significantly milder or altogether different nature than suggested by the 2MASS or near-infrared data alone. Hence, it is difficult to precisely quantify the number of IRTF confirmed versus potential 2MASS excesses.

However, by bulk, of the 27 suggested 2MASS candidate excesses, there are 17 white dwarfs in Table 2 with a confirmed or likely IRTF-measured excess. Interestingly, 10 of these are sufficiently mild that $(J - K)_{\text{IRTF}} < 0.3$ or $(J - H)_{\text{IRTF}} < 0.2$, and required shorter wavelength data to be recognized with confidence. Five additional sources display relatively strong IRTF excesses in all three near-infrared bandpasses; arising from low mass stellar companions, these five objects are also fairly unambiguous in

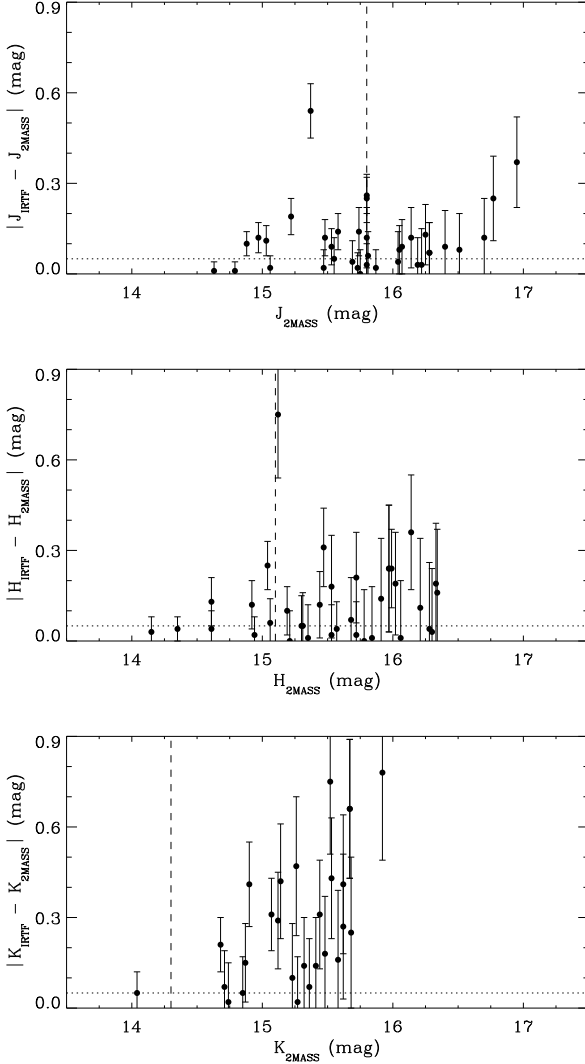


Figure 1. The absolute value of the magnitude difference between the IRTF and 2MASS near-infrared photometry for all mutually observed target stars, plotted versus magnitude and uncorrected for distinct filter sets. The displayed error bars are the 2MASS uncertainties, the dashed line represents the 2MASS 10σ detection threshold, and the dotted line represents a 5% error in the IRTF photometry.

2MASS, where they suffer from low S/N H - and K_s -band fluxes or source confusion. Figure 2 graphically represents all the IRTF near-infrared excesses, including the milder and more subtle cases, by plotting the 2MASS versus IRTF $J - H$ and $J - K$ measured colors for all white dwarfs with photometry in both datasets. As a rule, the plots show that the 2MASS data overpredicts the IRTF colors, especially in $J - K$, and that nine of 22 white dwarfs have $(J - K)_{\text{IRTF}} > 0.3$ as measured by the IRTF and 2MASS respectively.

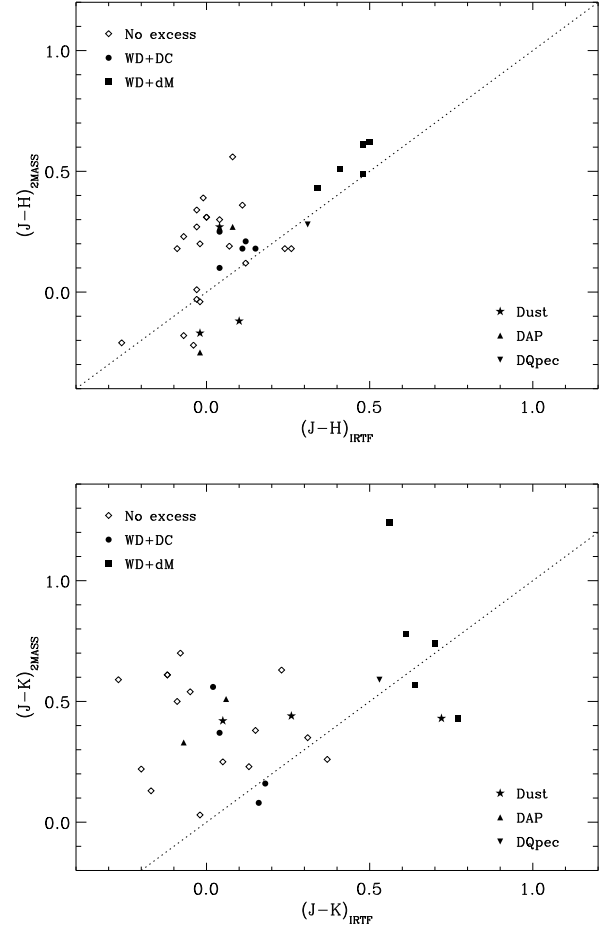


Figure 2. IRTF versus 2MASS near-infrared colors. The upper figure plots $J - H$ for all 37 white dwarfs in common, while the lower figure plots $J - K$ for all 30 white dwarfs in common. Objects with a confirmed or likely near-infrared excess are shown as filled symbols; error bars are not shown to avoid overcrowding in the figure.

5.2 Several Varieties of Near-Infrared Excess at White Dwarfs

Three metal-contaminated white dwarfs with dust disks and mid-infrared excess emission also display excess flux in the IRTF dataset: GD 16, GD 56 and PG 1457–086 (Farihi et al. 2009; Jura et al. 2007). Of the known white dwarfs with orbiting dust and an infrared excess, only about half reveal themselves shortward of $3 \mu\text{m}$ (Farihi et al. 2009; Kilic et al. 2006), and, where present, these near-infrared data constrain the inner dust temperature (Jura et al. 2009). Nine other metal-polluted white dwarfs have IRTF data consistent with photospheric emission, all of which have published or pending *Spitzer* IRAC observations.

Near-infrared excess due to cool, unevolved dwarf companions is typically evident and strong already by $1 \mu\text{m}$ (Farihi et al. 2005). Yet nearly all five white dwarf - red dwarf binaries confirmed by the IRTF observations had uncertain 2MASS photometric excesses which required more accurate measurements, primarily to obtain the $I - K$ color of the companion, which in turn constrains spectral type

(and mass for a given metallicity). A few cases were followed up in order to obtain higher spatial resolution images (Farihi et al. 2006) than are available via the 2MASS image server.

Few double white dwarf binaries are identified in the near-infrared, but such discoveries are not unprecedented (Farihi et al. 2005; Nelemans et al. 2005; Zuckerman et al. 1997). The cooler component in a double degenerate binary should be outshone by its primary at all wavelengths, in the ultraviolet and optical due to effective temperature, and in the infrared owing to radius. The component with an older cooling age should have finished the main sequence first, descending from the higher mass progenitor star, and becoming the higher mass and smaller radius degenerate star (Dobbie et al. 2006). These systems can still exhibit an excess from the smaller, cooler component, as can be seen for G158-78 and G53-38, where companions have been indicated by independent means. The IRTF photometry tentatively identifies three more double degenerate suspects: G62-46, GD 231, and GD 402.

The near-infrared data on the confirmed or likely magnetic DA white dwarfs KPD 0253+508 and KUV 2316+123, and DQp white dwarfs LHS 2293 and LP 494-12 range from surprising to spectacular. These stars are all presumably single at present, at least until shown otherwise. Non-interacting stellar and substellar companions to magnetic white dwarfs are rare (or possibly nonexistent; Liebert et al. 2005b), but that leaves room for a degenerate companion, as is suspected in the case of G62-46. In any case, non-magnetic models clearly fail to reproduce the spectral energy distributions of these stars – the near-infrared fluxes in particular – while magnetic models are lacking. The newly acquired IRTF data provides a new impetus to understand magnetic white dwarf atmospheres, which are still poorly constrained, especially in the infrared. Follow up spectroscopy is warranted for these cases, ideally with broad wavelength coverage from short optical wavelengths through the near-infrared.

ACKNOWLEDGMENTS

The author thanks referee T. Von Hippel for comments which improved the quality and clarity of the manuscript, D. Koester for the use of his models (and B. Gänsicke for providing them), M. Burleigh for many helpful discussions, A. Gianninas and G. Schmidt for sharing their optical spectra of PG 0939+071 and LHS 2293, respectively. The data presented here were obtained at the Infrared Telescope Facility, which is operated by the University of Hawaii under Cooperative Agreement no. NCC 5-538 with NASA, Science Mission Directorate, Planetary Astronomy Program. This publication makes use of data products from the Two Micron All Sky Survey, which is a joint project of the University of Massachusetts and the Infrared Processing and Analysis Center / California Institute of Technology, funded by NASA and the National Science Foundation. This work includes data taken with the NASA Galaxy Evolution Explorer, operated for NASA by the California Institute of Technology under NASA contract NAS5-98034. Some data presented herein are part of the Sloan Digital Sky Survey, which is managed

by the Astrophysical Research Consortium for the Participating Institutions (<http://www.sdss.org/>).

REFERENCES

- Adelman-McCarthy, J. K., et al. 2008, *ApJS*, 175, 297
 Becklin, E. E., Zuckerman, B. 1988, *Nature*, 336, 656
 Beauchamp, A., Wesemael, F., Bergeron, P., Fontaine, G., Saffer, R. A., Liebert, J., Brassard, P. 1999, *ApJ*, 516, 887
 Bergeron, P., Greenstein, J. L., Liebert, J. 1990, *ApJ*, 361, 190
 Bergeron, P., Leggett, S. K., Ruiz, M. T. 2001, *ApJS*, 133, 413
 Bergeron, P., Ruiz, M. T., Leggett, S. K. 1993, *ApJ*, 407, 733
 Bergeron, P., Ruiz, M. T., Leggett, S. K. 1997, *ApJS*, 108, 339
 Bergeron, P., Saffer, R. A., Liebert, J. 1992, *ApJ*, 394, 228
 Bergeron, P., Saumon, D., Wesemael, F. 1995a, *ApJ*, 443, 764
 Bergeron, P., Wesemael, F., Beauchamp, A. 1995b, *PASP*, 107, 1047
 Bochanski, J. J., West, A. A., Hawley, S. L., Covey, K. R. 2007, *AJ*, 133, 531
 Burleigh, M. R., Barstow, M. A. 1998, *MNRAS*, 295, L15
 Burleigh, M. R., Farihi, J., Napiwotzki, R., Marsh, T. R., Dobbie, P. D. 2009, *MNRAS*, submitted
 Burleigh, M. R. et al. 2008, *MNRAS*, 386, L5
 Carpenter, J. M. 2001, *AJ*, 121, 2851
 Copenhagen University Observatory 2006, *The Carlsberg Meridian Catalog 14* (Strasbourg: CDS)
 Catalán, S., Isern, J., García-Berro, E., Ribas, I., Allende-Prieto, C., Bonanos, A. Z. 2008, *A&A*, 477, 213
 Cushing, M. C., Vacca, W. D., Rayner, J. T. 2004, *PASP*, 116, 362
 DENIS Consortium 2005, *The DENIS Database, 3rd Release* (Strasbourg: CDS)
 Dobbie, P. D., et al. 2006, *MNRAS*, 369, 383
 Downes, R. A., Margon, B. 1983, *PASP*, 95, 358
 Dreizler, S., Werner, K. 1996, *A&A*, 314, 217
 Dufour, P., et al. 2007, *ApJ*, 663, 1291
 Dupuis, J., Fontaine, G., Wesemael, F. 1993b, *ApJS*, 87, 345
 Eggen, O. J. 1968, *ApJS*, 16, 97
 Eggen, O. J., Greenstein, J. L. 1965, *ApJ*, 142, 925
 Eisenstein, D. J., et al. 2006, *AJ*, 132, 676
 Farihi, J., Becklin, E. E., Zuckerman, B. 2005a, *ApJS*, 161, 394
 Farihi, J., Becklin, E. E., Zuckerman, B. 2008a, *ApJ*, 681, 1470
 Farihi, J., Hoard, D. W., Wachter S. 2006, *ApJ*, 646, 480
 Farihi, J., Jura, M., Zuckerman, B. 2009, *ApJ*, 694, 805
 Farihi, J., Zuckerman, B., & Becklin, E. E. 2008b, *ApJ*, 674, 431
 Green, P. J., Ali, B., Napiwotzki, R. 2000, *ApJ*, 540, 992
 Green, R. F., Schmidt, M., Liebert, J. 1986, *ApJS*, 61, 305
 Greenstein, J. L. 1984, *ApJ*, 276, 602
 Greenstein, J. L., Liebert, J. W. 1990, *ApJ*, 360, 662
 Hagen H. J., Groote D., Engels D., Haug U., Toussaint, F., Reimers, D. 1987, *A&A*, 183, L7

Table 3. Constraints on Multiple System Components

WD	Companion	Spectral Type	Separation (arcsec)	d (pc)
0023–109	G158-78B	dM0	59.4	92
	G158-78C	DC8
0235+064	PG 0235+064B	dM3.5	7.8	62
0257–005	KUV 0257–005B	dM4.5	1.0	494
0518+333	G86-B1AC	dM3	7.4	65
0956+045	PG 0956+045B	dM5	2.0	114
1013–010	G53-38B	DC8
1108+325	TON 60B	dM3	0.2	560
1133+489	PG 1133+489B	dM5	0.1	370
1140+004	WD 1140+004B	dM5	...	240
1619+525	1619+525B	dM2	2.6	300
	1619+525C	dM5	0.5	300

- Holberg, J. B., Sion, E. M., Oswalt, T., McCook, G. P., Foran, S., Subasavage, J. P. 2008, *AJ*, 135, 1225
- Homeier, D., Koester, D., Hagen, H. J., Jordan, S., Heber, U., Engels, D., Reimers, D., Dreizler, S. 1998, *A&A*, 338, 563
- Jordan, S. 2001, Proceedings of the 12th European Workshop on White Dwarfs, eds. J. L. Provencal et al. (San Francisco: ASP), 269
- Jordan, S., Friedrich, S. 2002, *A&A*, 383, 519
- Jura, M., Farihi, J., Zuckerman, B. 2007a, *ApJ*, 663, 1285
- Jura, M., Farihi, J., Zuckerman, B. 2009, *AJ*, 137, 3191
- Kalirai, J. S., Hansen, B. M. S., Kelson, D. D., Reitzel, D. B., Rich, R. M., Richer, H. B. 2008, *ApJ*, 676, 594
- Kawka, A., Vennes, S. 2006, *ApJ*, 643, 402
- Kilic, M., Farihi, J., Nitta, A., Leggett, S. K. 2008, *AJ*, 136, 111
- Kilic, M., von Hippel, T., Leggett, S. K., Winget, D. E. 2006, *ApJ*, 646, 474
- Kilkenny, D., O'Donoghue, D., Koen, C., Stobie, R. S., Chen A. 1997, *MNRAS*, 287, 867
- Kirkpatrick, J. D., McCarthy, D. W. 1994, *AJ*, 107, 333
- Kleinman, S. J. et al. 2004, *ApJ*, 607, 426
- Koester, D. 2009, to appear in *Memorie della Societa Astronomica Italiana*, based on lectures given at the School of Astrophysics “F. Lucchin”, Tarquinia, June 2008 (arXiv:0812.048)
- Koester, D., et al. 2001, *A&A*, 378, 556
- Koester, D., Rollenhagen, K., Napiwotzki, R., Voss, B., Christlieb, N., Homeier, D., Reimers, D. 2005a, *A&A*, 432, 1025
- Koester, D., Napiwotzki, R., Voss, B., Homeier, D., Reimers, D. 2005b, *A&A*, 439, 317
- Liebert, J., Angel, J. R. P., Stockman, H. S., Beaver, E. A. 1978, *ApJ*, 225, 181
- Liebert, J., Schmidt, G. D., Sion, E. M., Starrfield, S. G., Green, R. F., Boroson, T. A. 1985, *PASP*, 97, 158
- Liebert, J., Bergeron, P., Holberg, J. B. 2003, *AJ*, 125, 348
- Liebert, J., Bergeron, P., Holberg, J. B. 2005, *ApJS*, 156, 47
- Liebert, J., et al. 2005, *AJ*, 129, 2376
- Lisker, T., Heber, U., Napiwotzki, R., Christlieb, N., Han, Z., Homeier, D., Reimers, D. 2005, *A&A*, 430, 223
- Massey, P., Johnson, K. E., Degioia-Eastwood K. 1995, *ApJ*, 454, 151
- McCook, G. P., Sion, E. M. 2006, *Catalog of Spectroscopically Identified White Dwarfs* (Strasbourg: CDS)
- McCook, G. P., Sion, E. M. 1999, *ApJS*, 121, 1
- Monet, D., et al. 2003, *AJ*, 125, 984
- Morales-Rueda, L., Marsh, T. R., Maxted, P. F. L., Nelemans, G., Karl, C., Napiwotzki, R., Moran, C. K. J. 2005, *MNRAS*, 359, 648
- Napiwotzki, R., Green, P. J., Saffer, R. A. 1999, *ApJ*, 517, 399
- Nelemans, G., et al. 2005, *A&A*, 440, 1087
- Pauli, E. M., Napiwotzki, R., Heber, U., Altmann, M., Odenkirchen, M. 2006, *A&A*, 447, 173
- Probst, R. 1983, *ApJS*, 53, 335
- Putney, A. 1997, *ApJS*, 112, 527
- Raymond, S. N., et al. 2003, *AJ*, 125, 2621
- Rayner, J. T., Toomey, D. W., Onaka, P. M., Denault, A. J., Stahlberger, W. E., Vacca, W. D., Cushing, M. C., Wang S. 2003, *PASP*, 115, 362
- Rebassa-Mansergas, A., Gänsicke, B. T., Rodríguez-Gil, P., Schreiber, M. R., Koester, D. 2007, *MNRAS*, 382, 1377
- Reid, I. N. 1996, *AJ*, 111, 2000
- Salim, S., Gould, A. 2003, *ApJ*, 582, 1011
- Schmidt, G. D., Smith, P. S. 1994, *ApJ*, 423, L63
- Schmidt, G. D., Bergeron, P., Fegley, B. 1995, *ApJ*, 443, 274
- Schmidt, G. D., Liebert, J., Harris, H. C., Dahn, C. C., Leggett, S. K. 1999, *ApJ*, 512, 916
- Silvestri, N. M., et.al. 2006, *AJ*, 131, 1674
- Sion, E. M., Hammond, G. L., Wagner, R. M., Starrfield, S. G., Liebert, J. 1990, *ApJ*, 362, 691
- Skrutskie, M. F., et al. 2006, *AJ*, 131, 1163
- Space Telescope Science Institute 2006, *The Guide Star Catalog Version 2.3*, (Baltimore: STScI)
- Steele, P. R., Burleigh, M. R., Farihi, J., Gänsicke, B. T., Jameson, R. F., Dobbie, P. D., Barstow Dobbie, M. A. 2009, *A&A*, in press
- Vacca, W. D., Cushing, M. C., Rayner, J. T. 2003, *PASP*, 115, 389
- van Altena, W. F., Lee, J. T., Hoffleit, E. D. 1995, *The General Catalogue of Trigonometric Parallaxes*, 4th edition (New Haven: Yale University Observatory)
- Vennes, S., Smith, R. J., Boyle, B. J., Croom, S. M., Kawka, A., Shanks, T., Miller, L., Loaring, N. 2002, *MNRAS*, 335, 673

- von Hippel, T., Kuchner, M. J., Kilic, M., Mullaly, F., & Reach, W. T. 2007, *ApJ*, 662, 544
- Voss, B., Koester, D., Napiwotzki, R., Christlieb, N., Reimers, D. 2007, *A&A*, 470, 1079
- Wachter, S., Hoard, D. W., Hansen, K. H., Wilcox, R. E., Taylor, H. M., Finkelstein, S. L. 2003, *ApJ*, 586, 1356
- Wellhouse, J. W., Hoard, D. W., Howell, S. B., Wachter, S., Esin, A. A. 2005, *PASP*, 117, 1378
- Williams, K. A., Bolte, M., Koester, D. 2009, *ApJ*, 693, 355
- Wolff, B., Koester, D., Liebert, J. 2002, *A&A*, 385, 995
- Zacharias, N., Urban, S. E., Zacharias, M. I., Wycoff, G. L., Hall, D. M., Monet, D. G., Rafferty, T. J. 2004 *AJ*, 127, 3043
- Zacharias, N., Monet, D. G., Levine, S. E., Urban, S. E., Gaume, R., Wycoff, G. L. 2005, *The NOMAD Catalog* (Strasbourg: CDS)
- Zuckerman, B., Becklin, E. E., Macintosh, B. A., Bida, T. 1997, *AJ*, 113, 764
- Zuckerman, B., Koester, D., Reid, I. N., Hünsch, M. 2003, *ApJ*, 596, 477
- Zuckerman, B., et al. 2008, *ApJ*, 683, 1085

APPENDIX A: INDIVIDUAL SPECTRAL ENERGY DISTRIBUTIONS

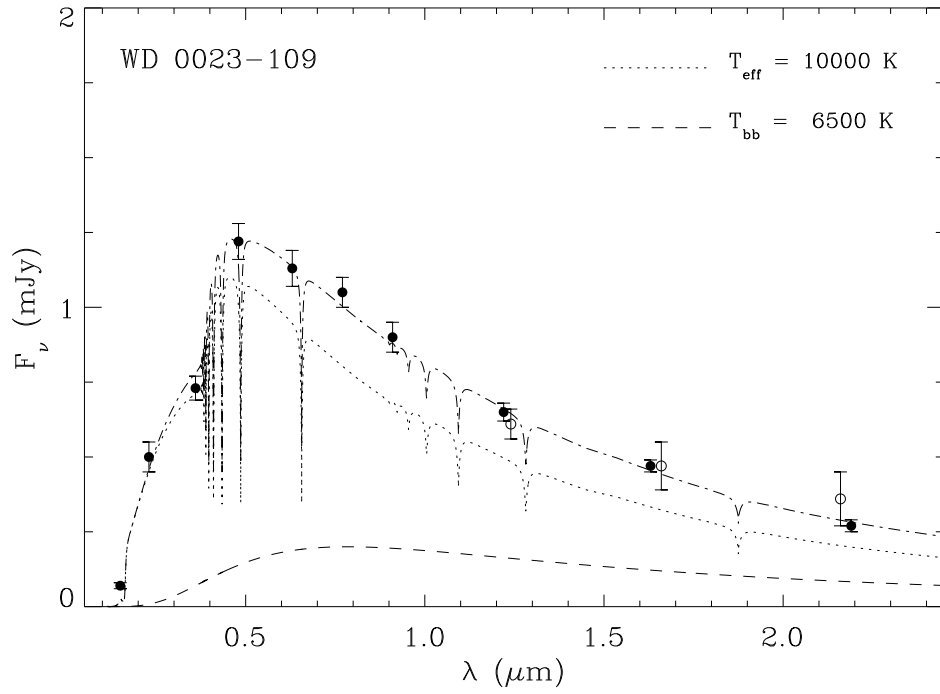


Figure A1. Spectral energy distribution of G158-78. The solid circles are *GALEX* far- and near-ultraviolet, SDSS *ugriz*, and IRTF *JHK* photometry, while the open circles are 2MASS *JHK_s* photometry. The star is a likely double degenerate.

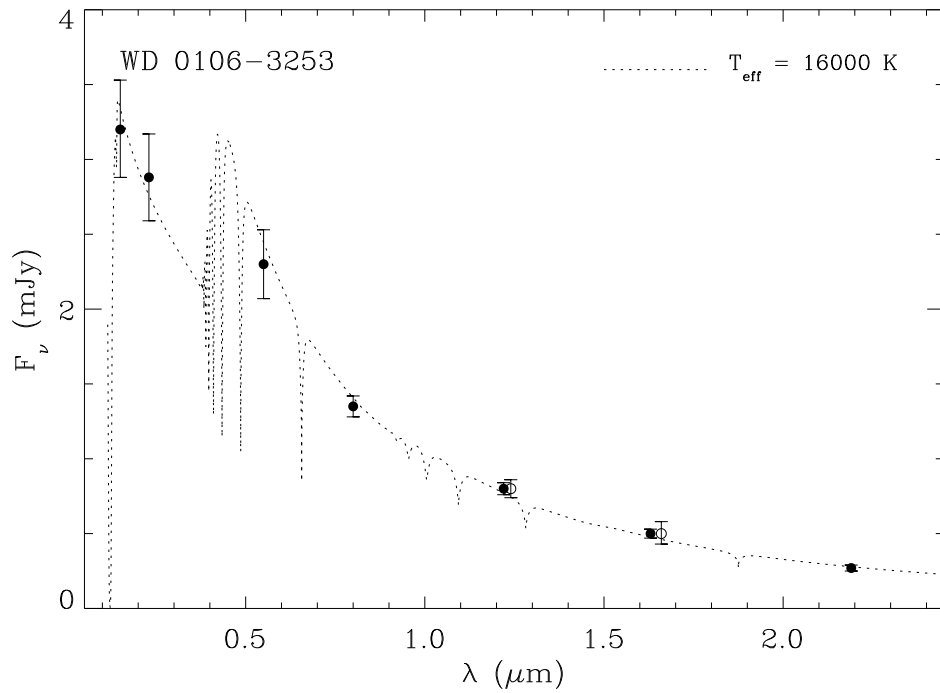


Figure A2. Spectral energy distribution of HE 0106-3253. The solid circles are *GALEX* far- and near-ultraviolet, optical *VI*, and IRTF *JHK* photometry, while the open circles are 2MASS *JH* photometry.

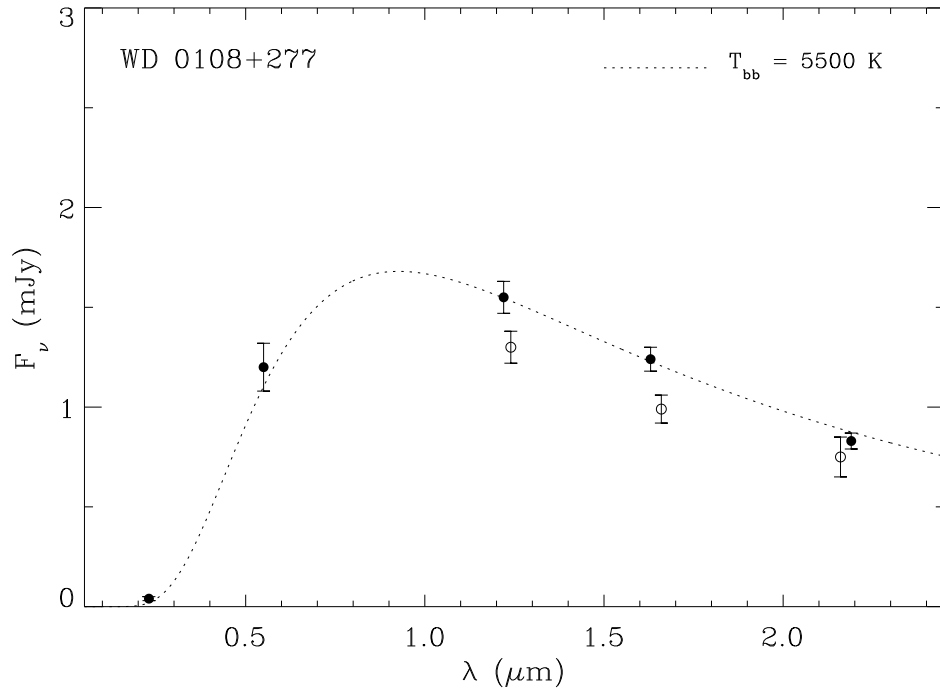


Figure A3. Spectral energy distribution of NLTT 3915. The solid circles are *GALEX* near-ultraviolet, optical *V*, and IRTF *JHK* photometry, while the open circles are 2MASS *JHK_s* photometry.

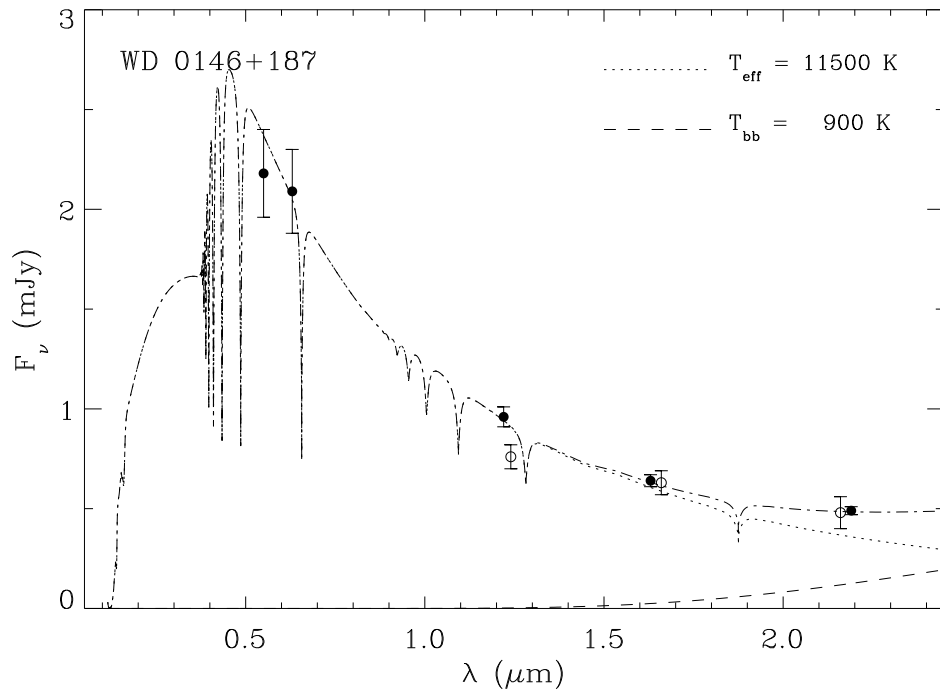


Figure A4. Spectral energy distribution of GD 16. The solid circles are optical *V_r*, and IRTF *JHK* photometry, while the open circles are 2MASS *JHK_s* photometry. There are no *GALEX* data available for this star.

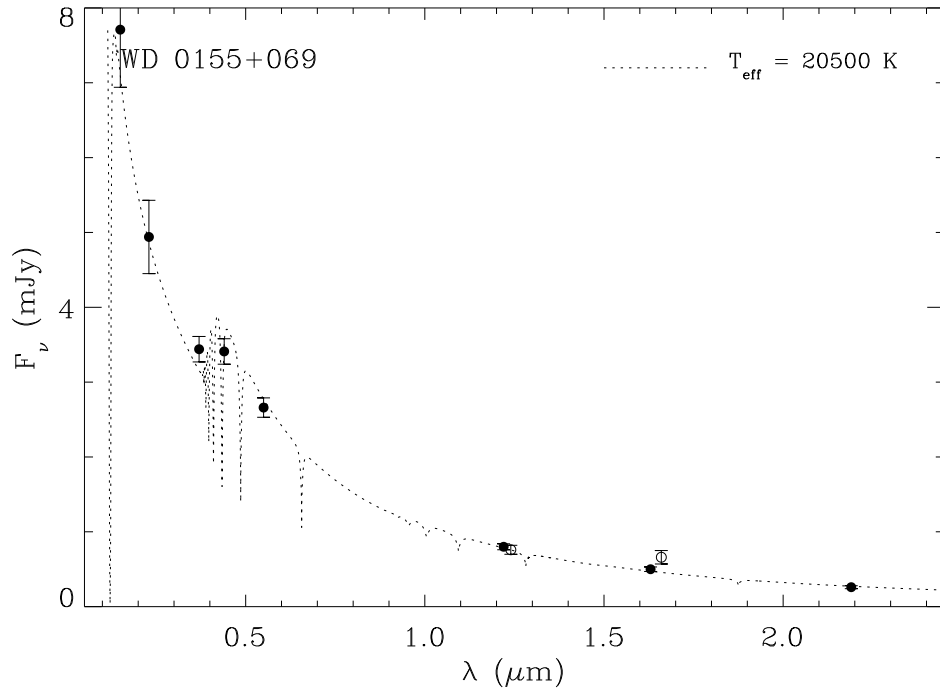


Figure A5. Spectral energy distribution of GD 20. The solid circles are *GALEX* far- and near-ultraviolet, optical *UBV*, and IRTF *JHK* photometry, while the open circles are 2MASS *JH* photometry.

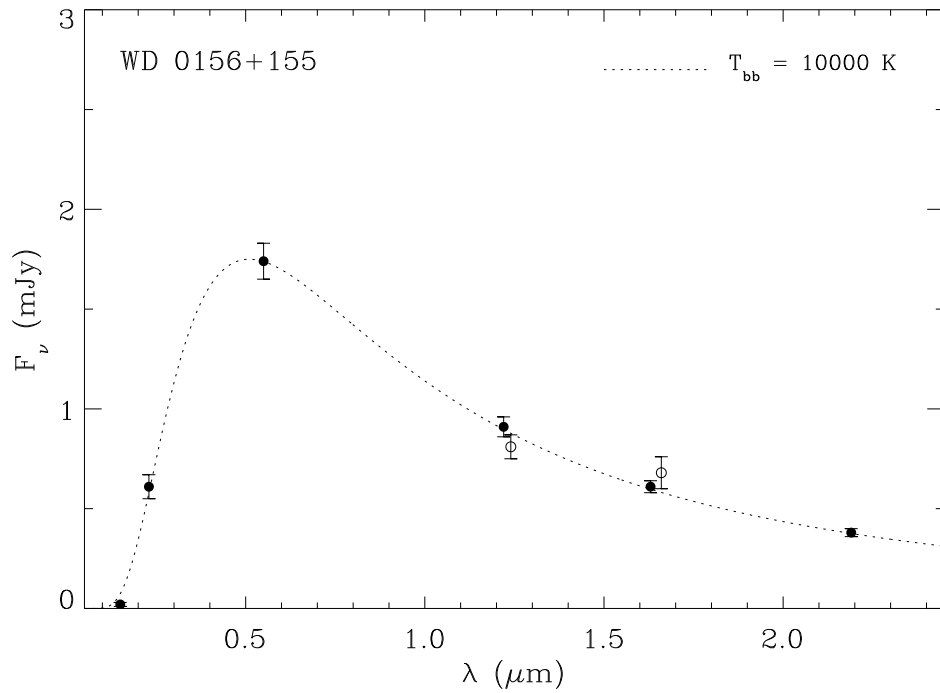


Figure A6. Spectral energy distribution of PG 0156+155. The solid circles are *GALEX* far- and near-ultraviolet, optical *V*, and IRTF *JHK* photometry, while the open circles are 2MASS *JH* photometry.

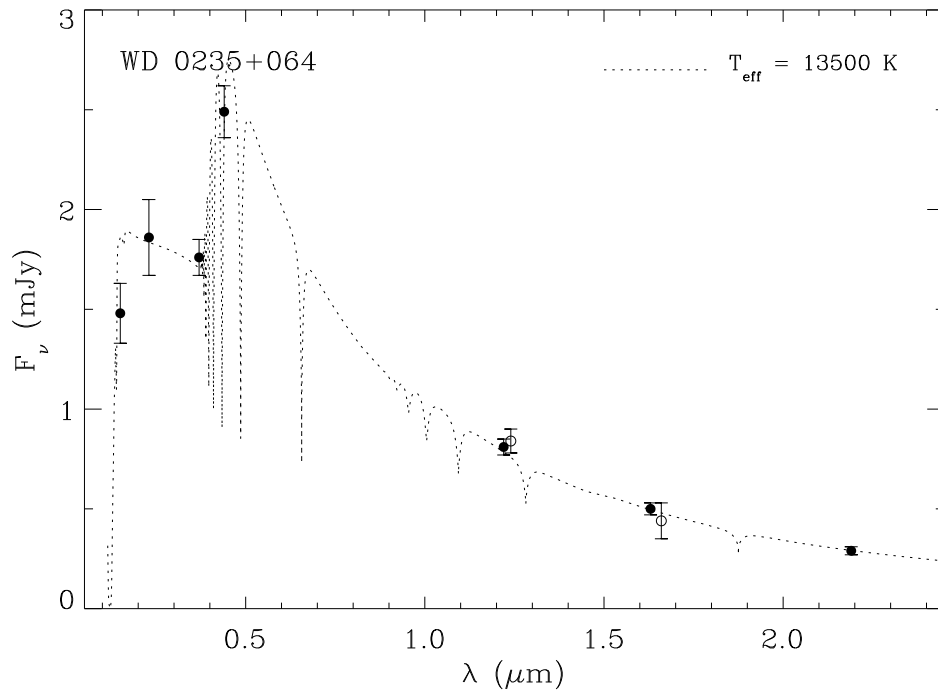


Figure A7. Spectral energy distribution of PG 0235+064. The solid circles are *GALEX* far- and near-ultraviolet, optical *UB*, and IRTF *JHK* photometry, while the open circles are 2MASS *JH* photometry. The solid-circle photometry is uncontaminated by the nearby common-proper motion companion (Farihi et al. 2008b), indicating a new, higher effective temperature for this white dwarf.

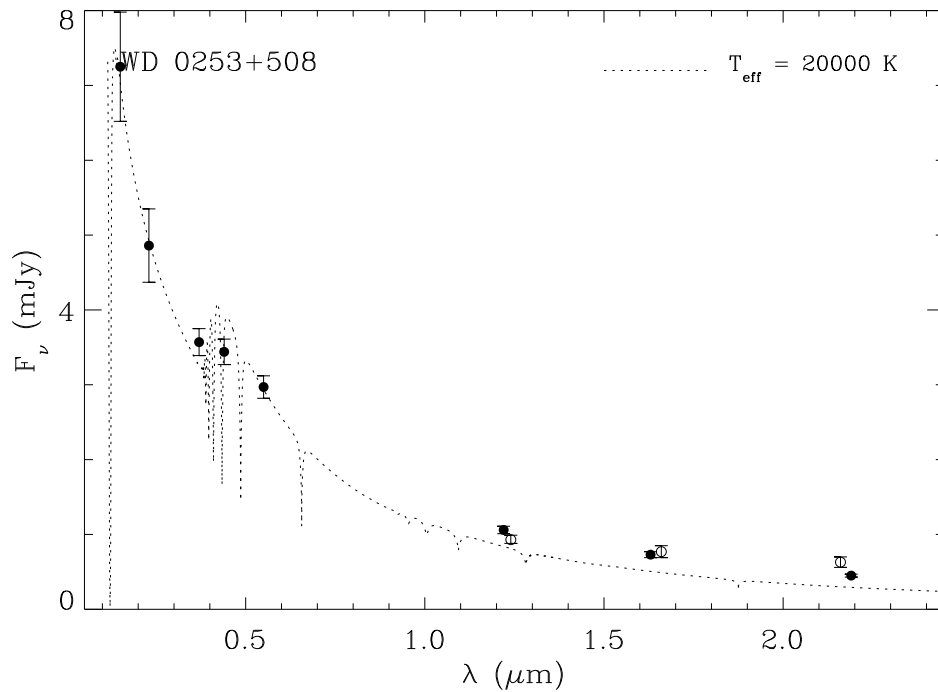


Figure A8. Spectral energy distribution of KPD 0253+508. The solid circles are *GALEX* far- and near-ultraviolet, optical *UBV*, and IRTF *JHK* photometry, while the open circles are 2MASS *JHK_s* photometry. A single effective temperature does not fit this magnetic white dwarf; it has clear excess (relative to non-magnetic DA models) emission at *JHK*.

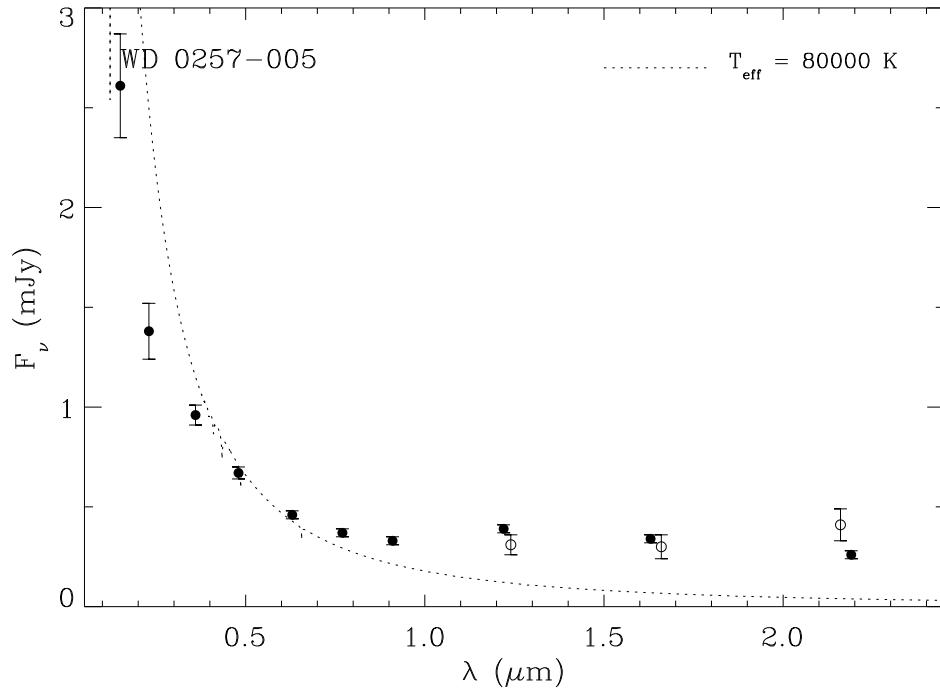


Figure A9. Spectral energy distribution of KUV 0257–005. The solid circles are *GALEX* far- and near-ultraviolet, SDSS *ugriz*, and IRTF *JHK* photometry, while the open circles are 2MASS *JHK_s* photometry. There is clear evidence for extinction at ultraviolet and optical wavelengths.

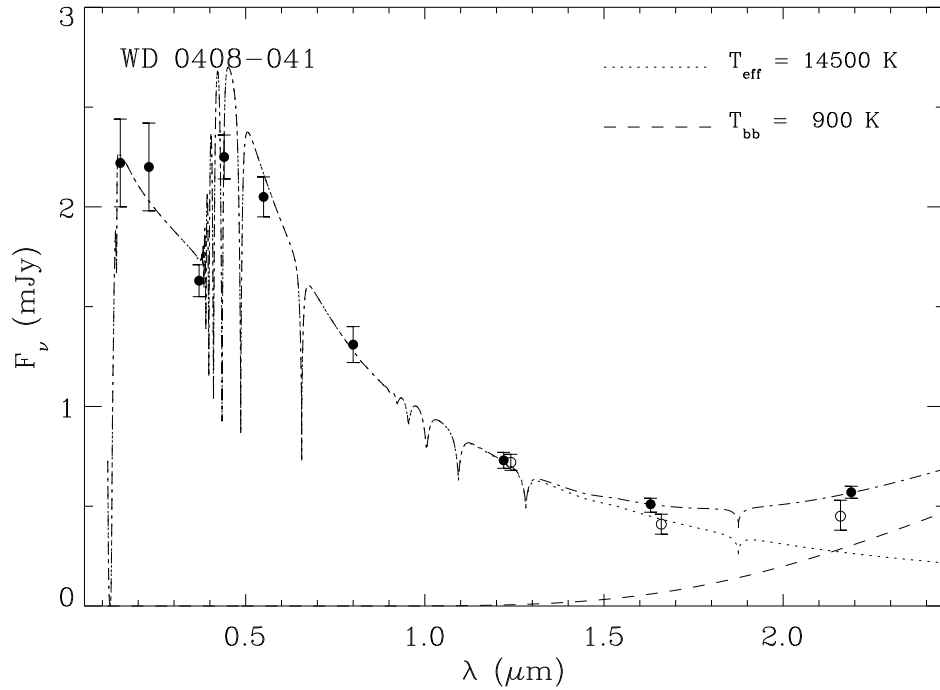


Figure A10. Spectral energy distribution of GD 56. The solid circles are *GALEX* far- and near-ultraviolet, optical *UBVI*, and IRTF *JHK* photometry, while the open circles are 2MASS *JHK_s* photometry.

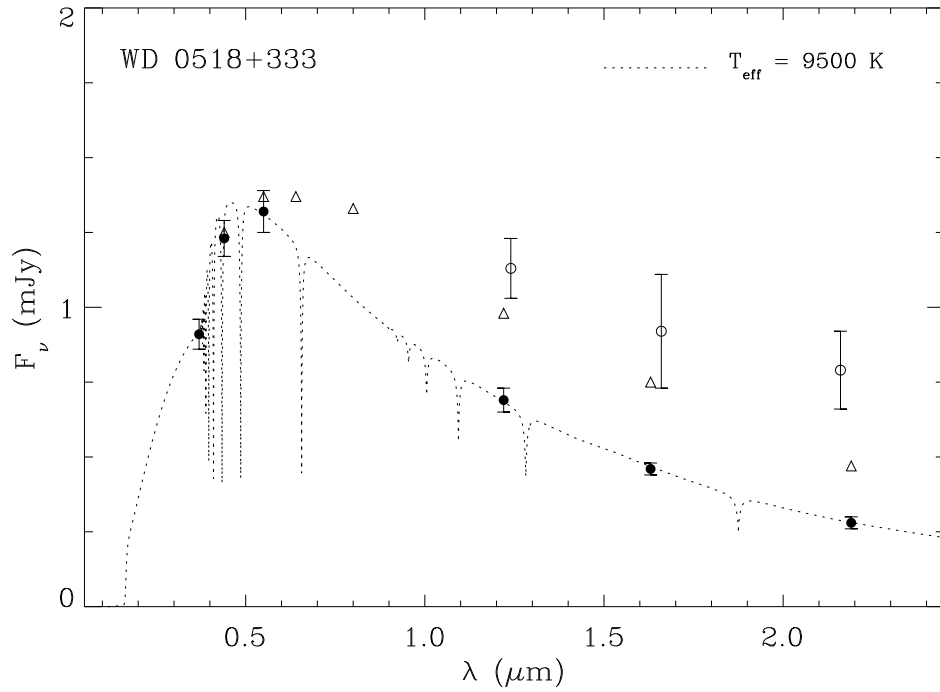


Figure A11. Spectral energy distribution of EG 43. The solid circles are optical $UBVI$, and IRTF JHK photometry, while the open circles are 2MASS JHK_s photometry, clearly contaminated by the light from the visual M dwarf companion. The open triangles are $BVR IJHK$ from Bergeron et al. (2001), also apparently contaminated at optical wavelengths.

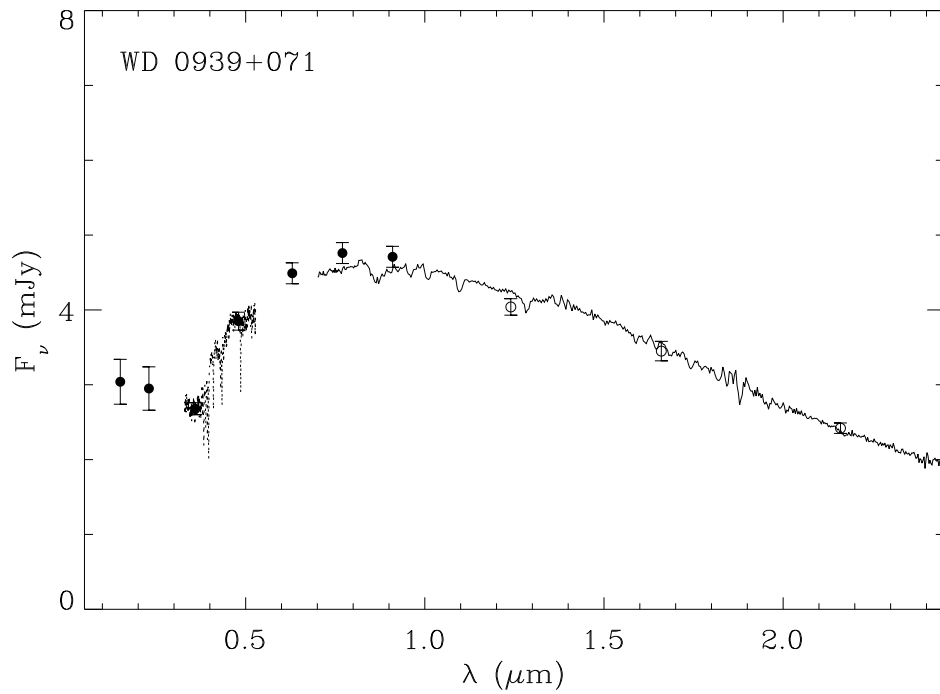


Figure A12. Spectral energy distribution of PG 0939+071. The solid circles are $GALEX$ far- and near-ultraviolet, and SDSS $ugriz$ photometry, while the open circles are 2MASS JHK_s photometry. The 0.7–2.5 μm spectrum was taken with SpeX, and the blue optical spectrum is also shown (see Figure A12).

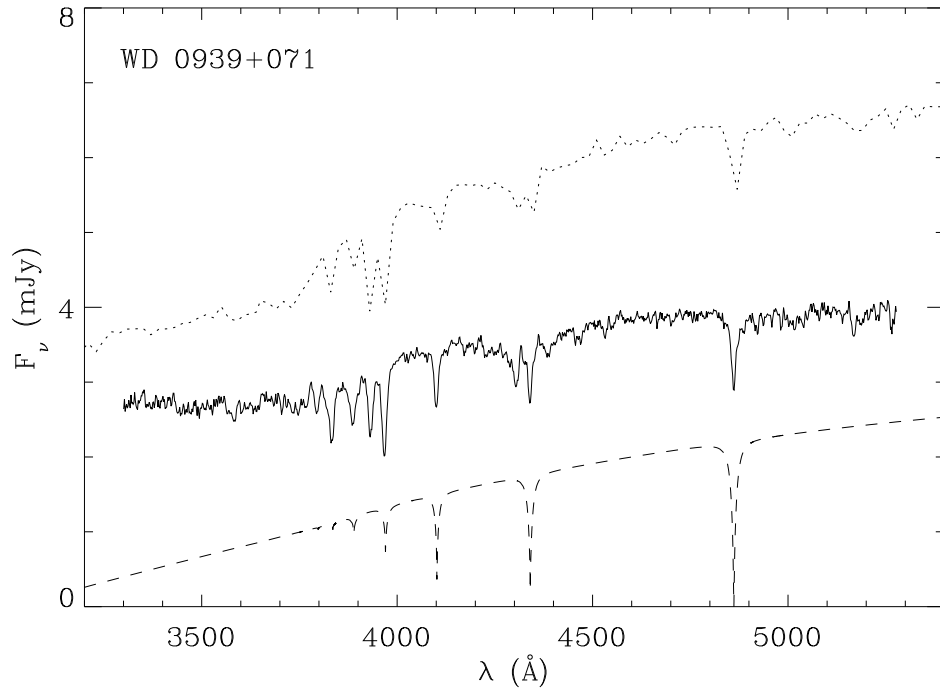


Figure A13. The blue optical spectrum of PG 0939+071 (A. Gianninas 2008, private communication), shown together with a 7000 K DA white dwarf model (dashed line), and a low resolution F2V stellar model (dotted line). Note the blue continuum in the actual data is not seen in either model.

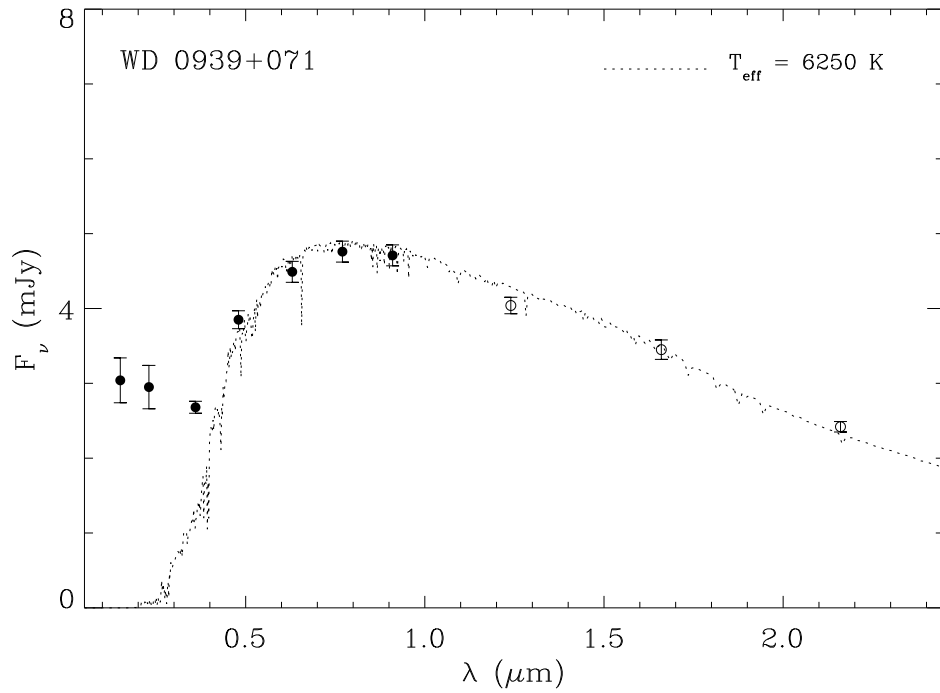


Figure A14. An F8V stellar model fitted to the optical and near-infrared photometry of PG 0939+071; revealing a clear ultraviolet flux excess.

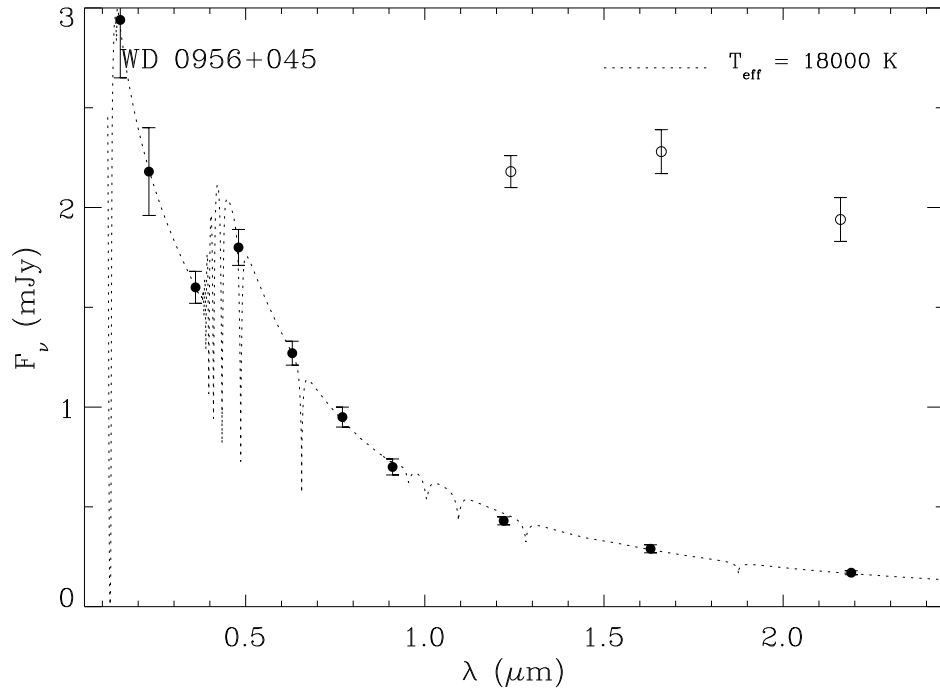


Figure A15. Spectral energy distribution of PG 0956+045A. The solid circles are *GALEX* far- and near-ultraviolet, SDSS *ugriz*, and IRTF *JHK* photometry. The open circles are 2MASS *JHK_s* photometry, which are primarily due to the flux from PG 0956+045B.

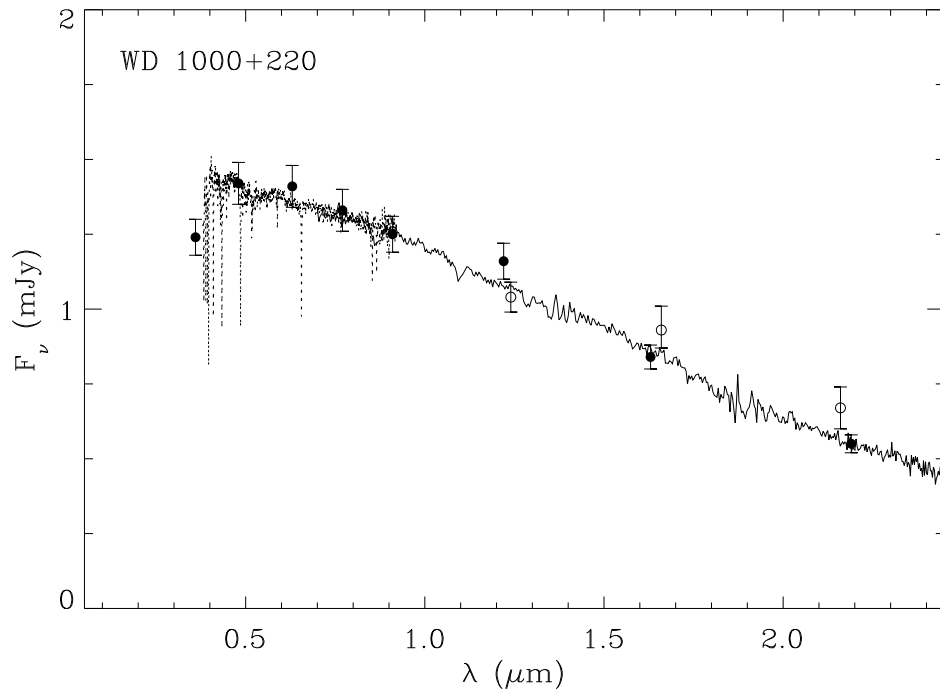


Figure A16. Spectral energy distribution of TON 1145. The solid circles are SDSS *ugriz*, and IRTF *JHK* photometry, while the open circles are 2MASS *JHK_s* photometry. The 0.7 – 2.5 μm spectrum was taken with SpeX, and the optical SDSS spectrum is also shown (see Figure A17).

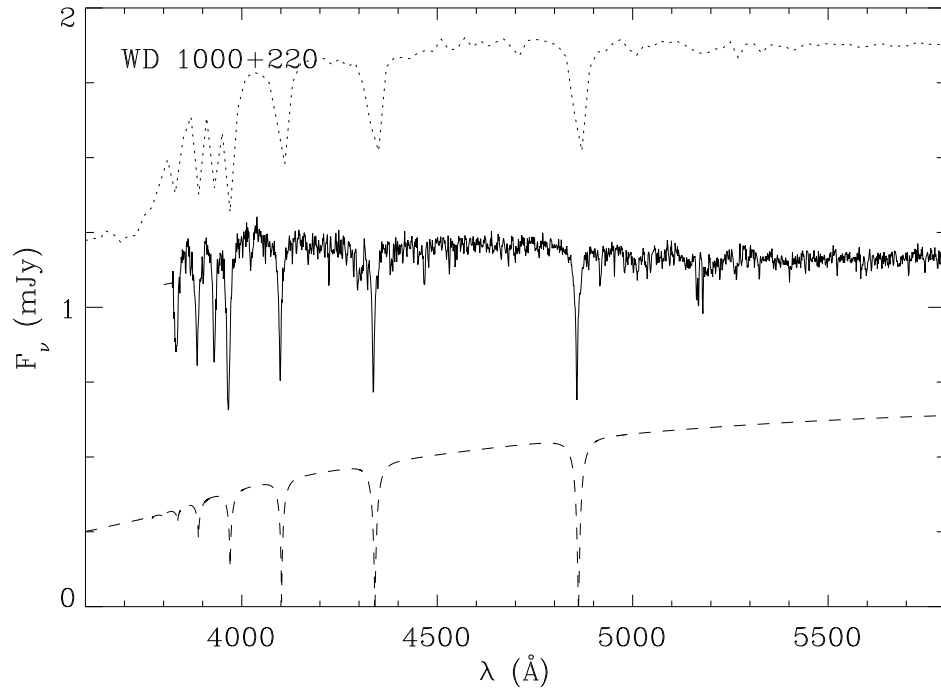


Figure A17. The SDSS blue optical spectrum of TON 1145, shown together with a 7500 K DA white dwarf model (dashed line), and a low resolution A8V stellar model (dotted line). Note the flat pseudo-continuum below 4500 \AA in the actual data is not seen in either model.

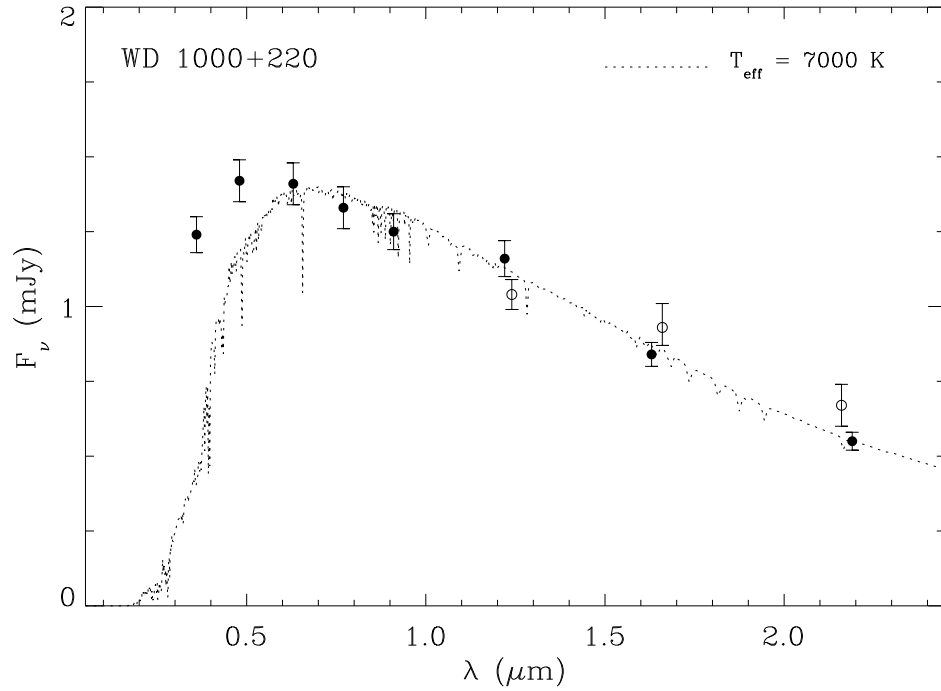


Figure A18. An F2V stellar model fitted to the optical and near-infrared photometry of TON 1145. While there are no *GALEX* data for this star, it appears possible it also has an ultraviolet excess.

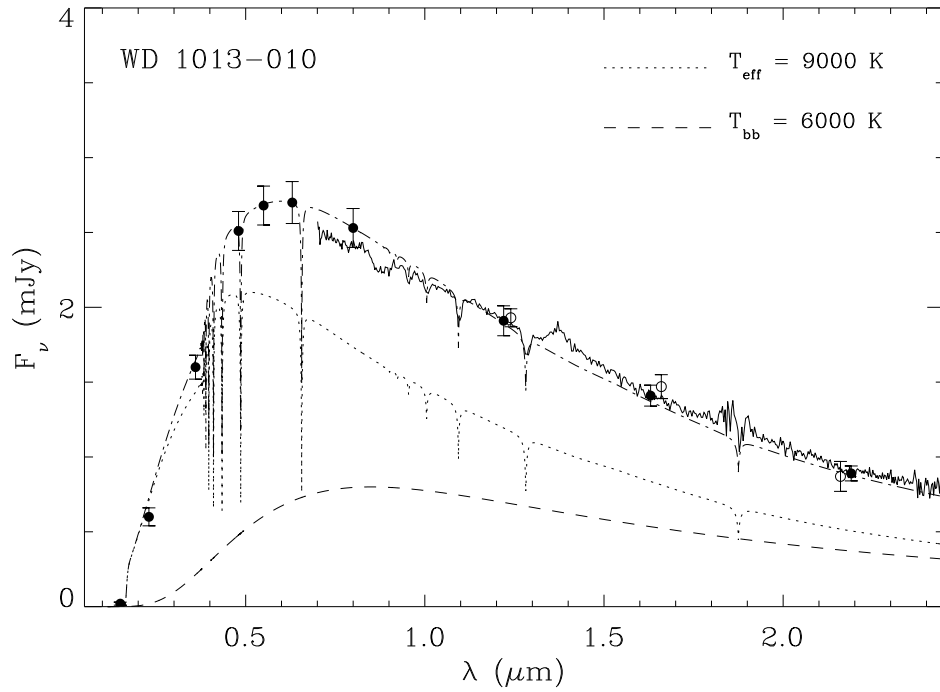


Figure A19. Spectral energy distribution of G53-38. The solid circles are *GALEX* far- and near-ultraviolet, SDSS *ugr*, optical *VI*, and IRTF *JHK* photometry, while the open circles are 2MASS *JHK_s* photometry. The 0.7 – 2.5 μm spectrum was taken with SpeX. There appears to be photometric evidence of the known, hidden white dwarf companion (Nelemans et al. 2005).

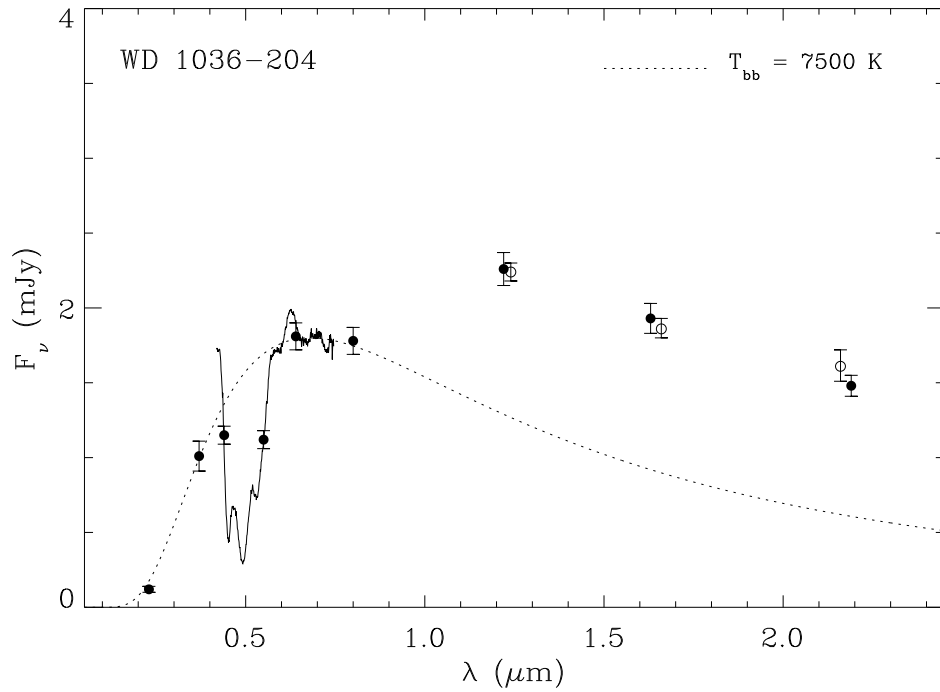


Figure A20. Spectral energy distribution of LHS 2293. The solid circles are *GALEX* near-ultraviolet, optical *UBVRI*, and IRTF *JHK* photometry, while the open circles are 2MASS *JHK_s* photometry. Also shown is the optical spectrum from Schmidt et al. (1995). The ultraviolet and optical photometry seem to indicate an effective temperature near 7500 K (Liebert et al. 1978).

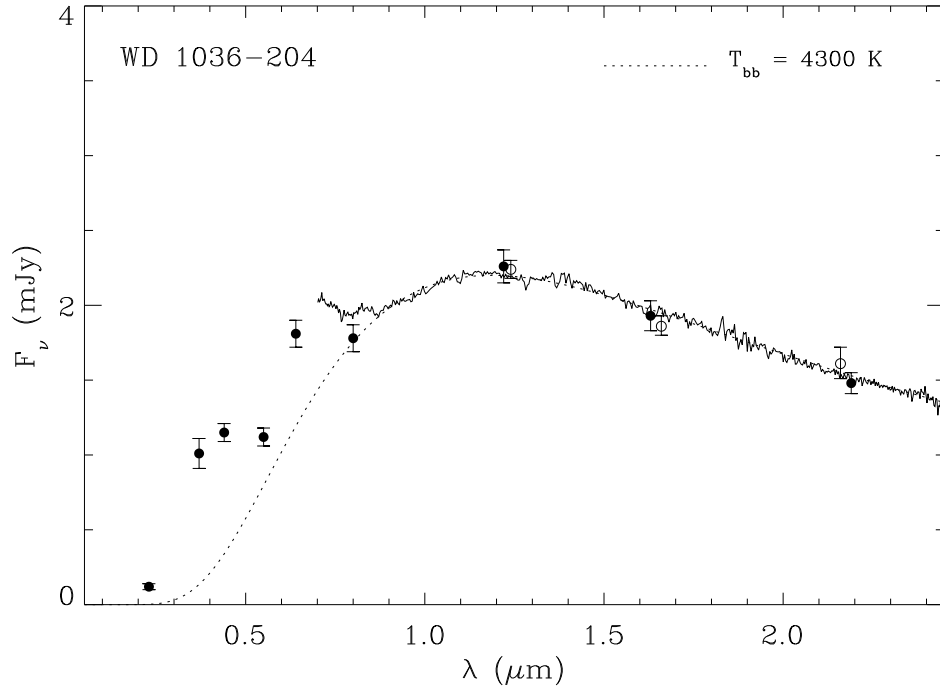


Figure A21. The $0.7 - 2.5 \mu\text{m}$ spectrum taken with SpeX indicates a significantly lower effective temperature of 4300 K. The region below $0.9 \mu\text{m}$ may suffer from poor correction to the instrument response.

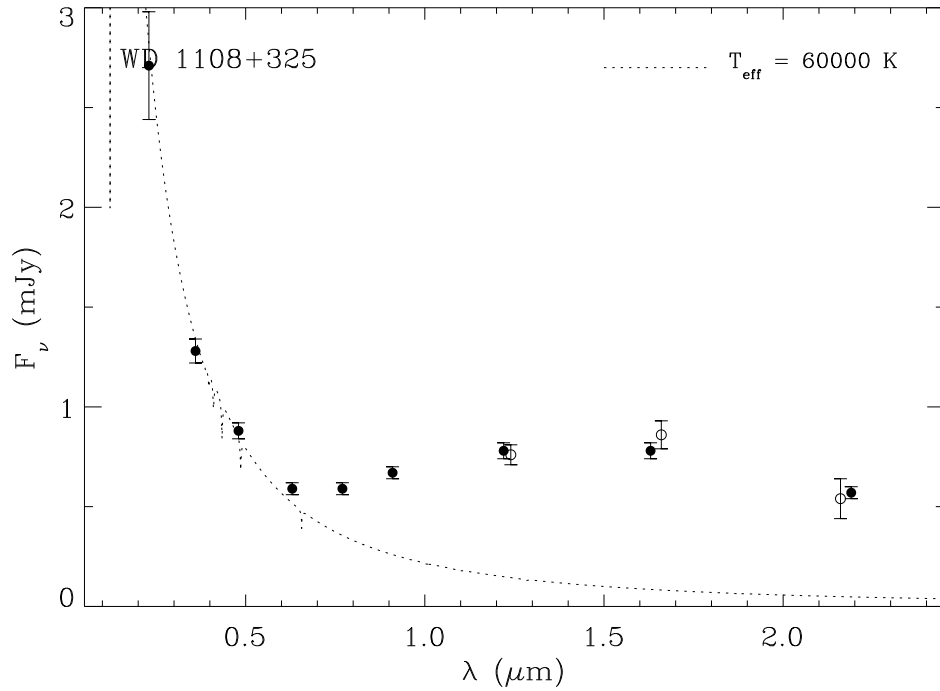


Figure A22. Spectral energy distribution of TON 60. The solid circles are *GALEX* near-ultraviolet, SDSS *ugriz*, and IRTF *JHK* photometry, while the open circles are 2MASS *JHK_s* photometry. The *GALEX* far-ultraviolet flux of $4.9 \pm 0.5 \text{ mJy}$ is not shown for scaling purposes. The light of TON 60B dominates at wavelengths beyond $0.8 \mu\text{m}$.

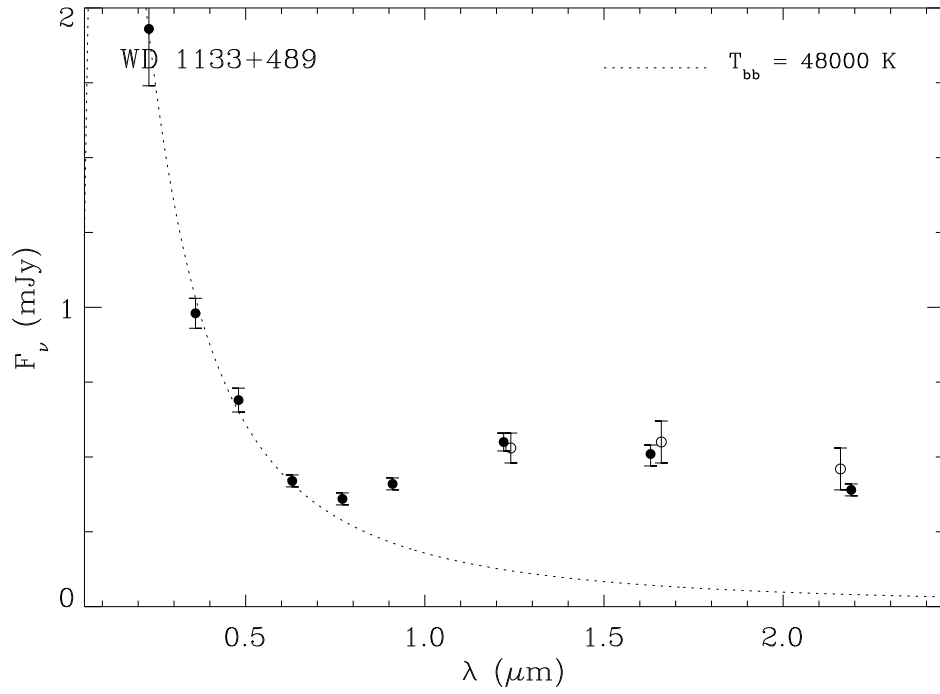


Figure A23. Spectral energy distribution of PG 1133+489. The solid circles are *GALEX* near-ultraviolet, SDSS *ugriz*, and IRTF *JHK* photometry, while the open circles are 2MASS *JHK_s* photometry. The *GALEX* far-ultraviolet flux of 3.1 ± 0.3 mJy is not shown for scaling purposes. The companion flux dominates at wavelengths beyond $0.8 \mu\text{m}$.

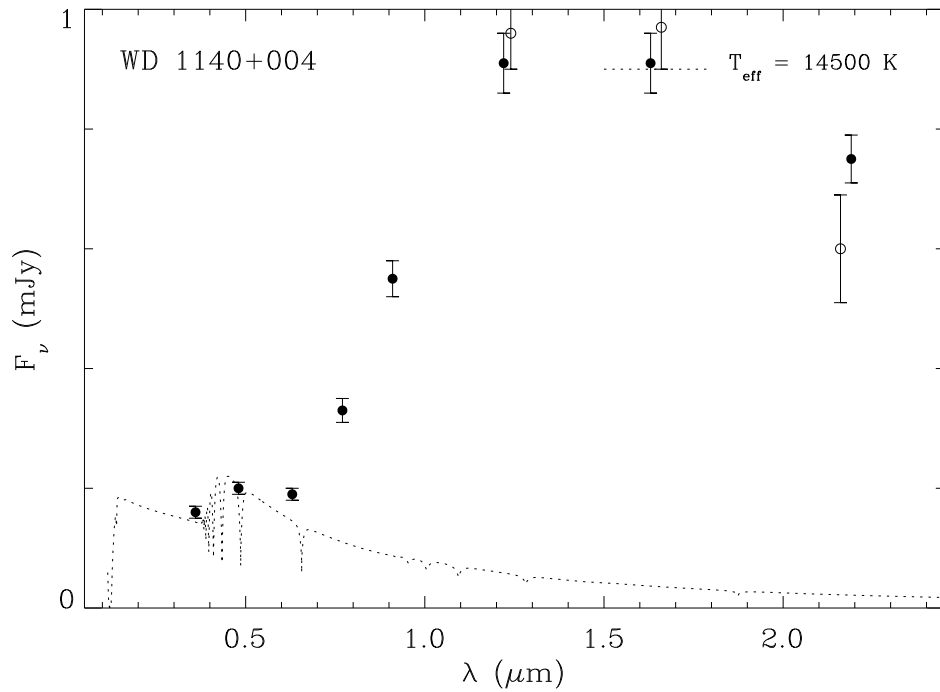


Figure A24. Spectral energy distribution of SDSS J114312.57+000926.5. The solid circles are SDSS *ugriz*, and IRTF *JHK* photometry, while the open circles are 2MASS *JHK_s* photometry. The *GALEX* data for this source appear unreliable due to a nearby, bright star. The companion flux strongly dominates the system at red optical wavelengths.

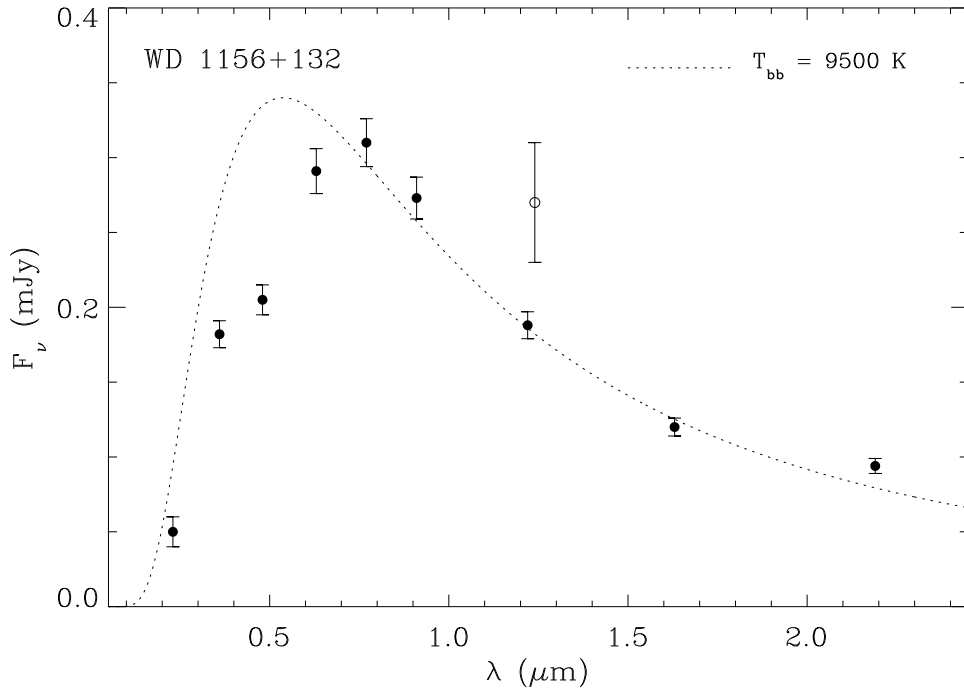


Figure A25. Spectral energy distribution of LP 494-12. The solid circles are *GALEX* near-ultraviolet, SDSS *ugriz*, and IRTF *JHK* photometry, while the open circle is 2MASS *J* photometry. The *ugr* flux points were ignored in the fit as large absorption bands affect those bandpasses, while the *iz* photometry is unaffected by features in the SDSS spectrum.

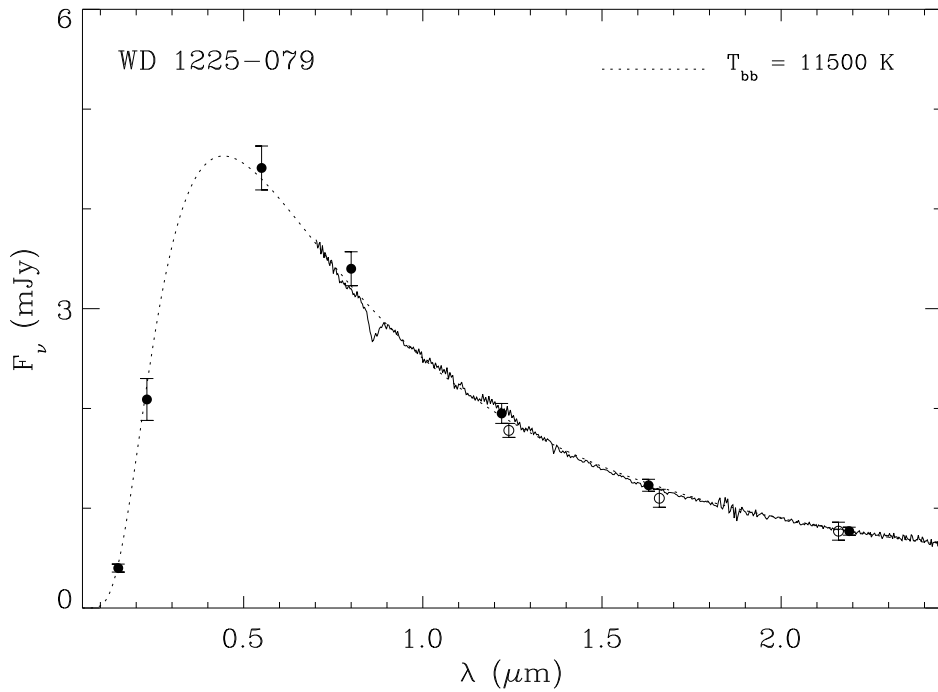


Figure A26. Spectral energy distribution of PG 1225-079. The solid circles are *GALEX* far- and near-ultraviolet, optical *V*, and IRTF *JHK* photometry, while the open circles are 2MASS *JHK_s* photometry. The 0.7 – 2.5 μm spectrum was taken with SpeX; the calcium absorption triplet centered near 8600 \AA is clearly detected.

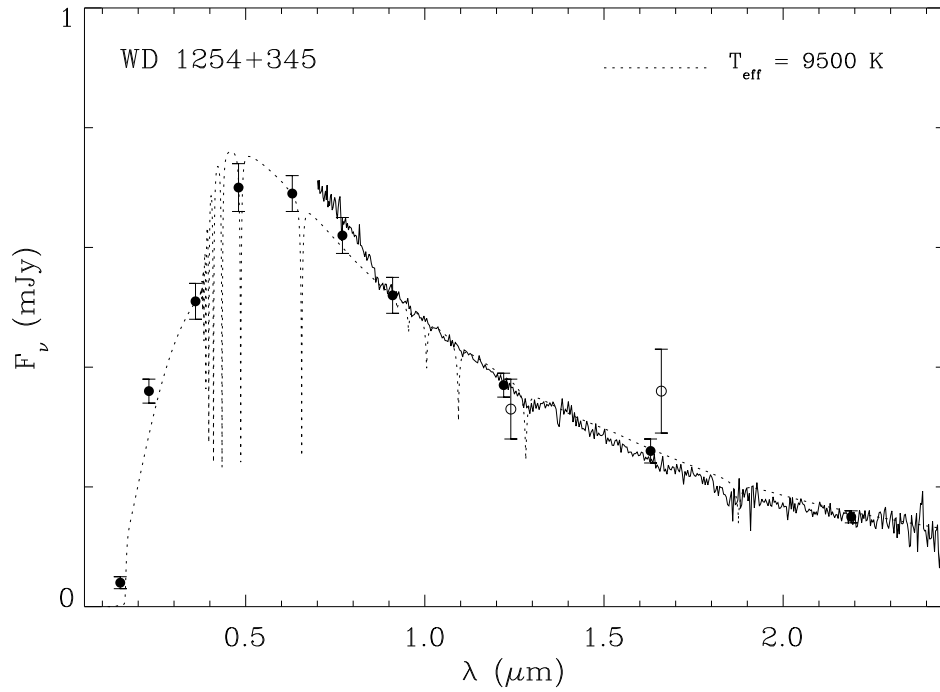


Figure A27. Spectral energy distribution of HS 1254+345. The solid circles are *GALEX* far- and near-ultraviolet, SDSS *ugriz*, and IRTF *JHK* photometry, while the open circles are 2MASS *JH* photometry. The 0.7–2.5 μm spectrum was taken with SpeX; the absence of hydrogen lines is consistent with the presence of a high magnetic field. The region below 0.9 μm may suffer from poor correction to the instrument response.

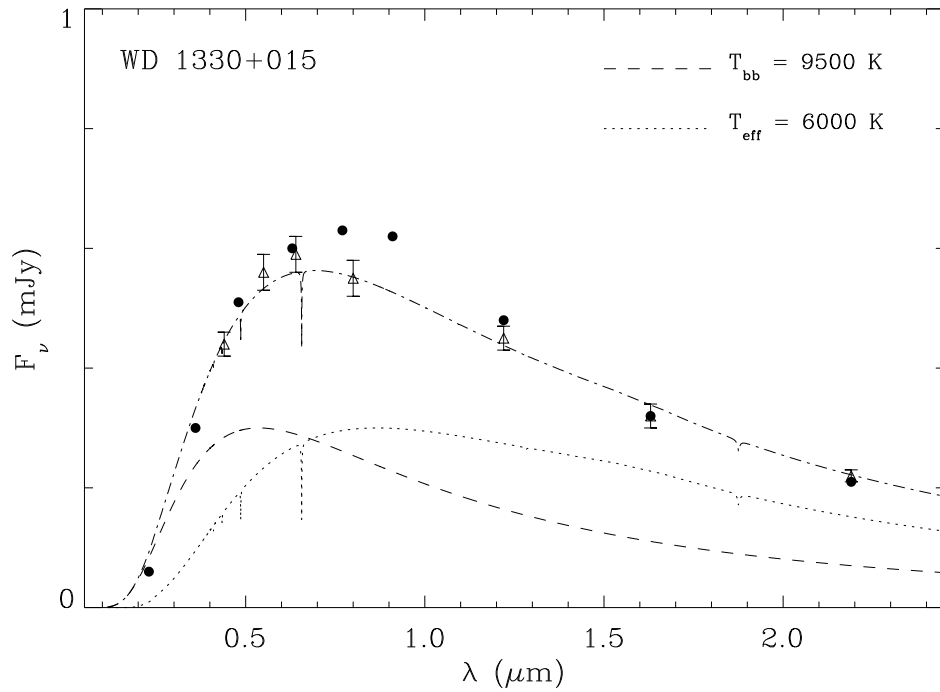


Figure A28. Spectral energy distribution of G62-46. The solid circles are *GALEX* near-ultraviolet, SDSS *ugriz*, and IRTF *JHK* photometry, while the open circles are 2MASS *JHK_s* photometry. The open triangles are *BVRIJHK* from Bergeron et al. (1997) and the models are fitted to their data. The *I*-band flux predicts a hotter DC component at odds with the SDSS *iz* photometry.

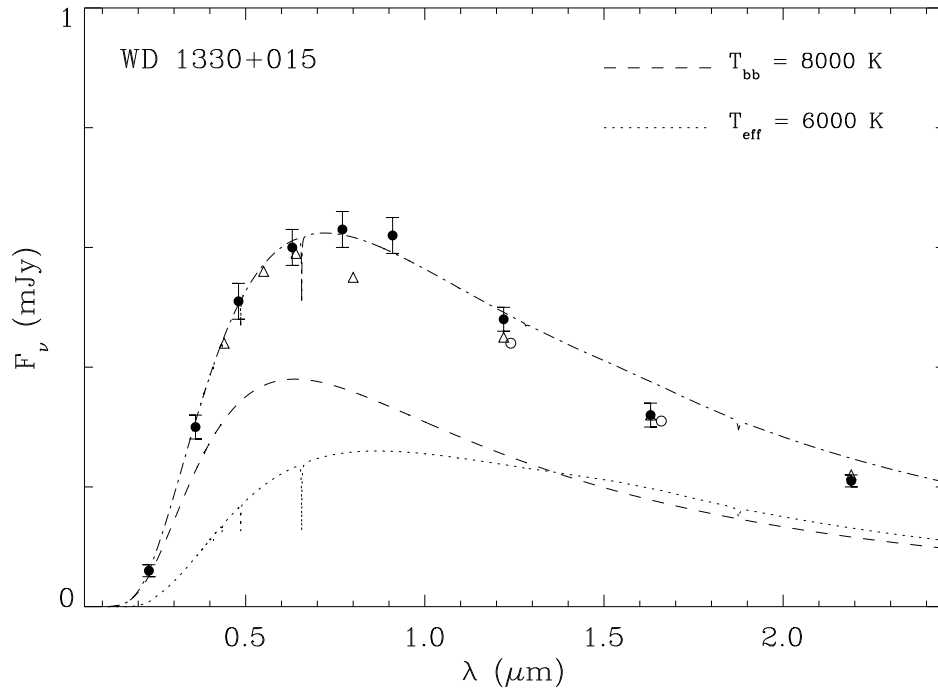


Figure A29. Same as Figure A28 but now the models are fitted to the *ugriz* photometry. While a cooler DC component reproduces the optical data, the full spectral energy distribution cannot be fitted simultaneously. Variability appears possible in this likely binary (see §4).

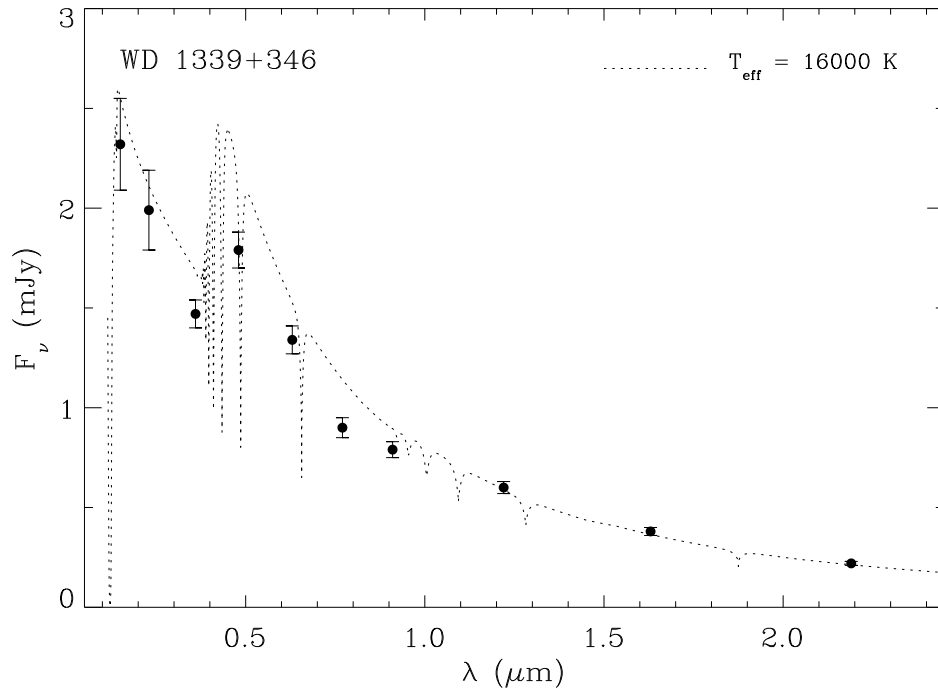


Figure A30. Spectral energy distribution of PG 1339+346. The solid circles are *GALEX* far- and near-ultraviolet, SDSS *ugriz*, and IRTF *JHK* photometry. The white dwarf was spatially and photometrically resolved from its apparent (i.e. non-physical) companion $2''.6$ away (see §4) during the IRTF observations, but the reliability of the SDSS photometry is uncertain. It appears that the *ugriz* photometry was adversely affected by the background star.

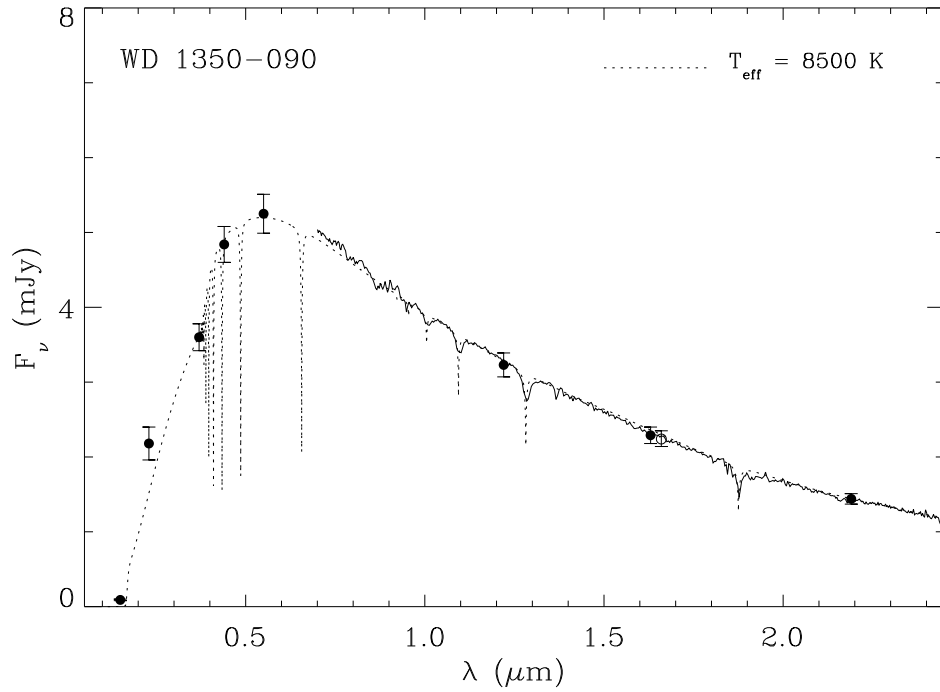


Figure A31. Spectral energy distribution of LP907-37. The solid circles are *GALEX* far- and near-ultraviolet, optical *UBV*, and IRTF *JHK* photometry, while the open circle is 2MASS *H* photometry. The 0.7 – 2.5 μm spectrum was taken with SpeX.

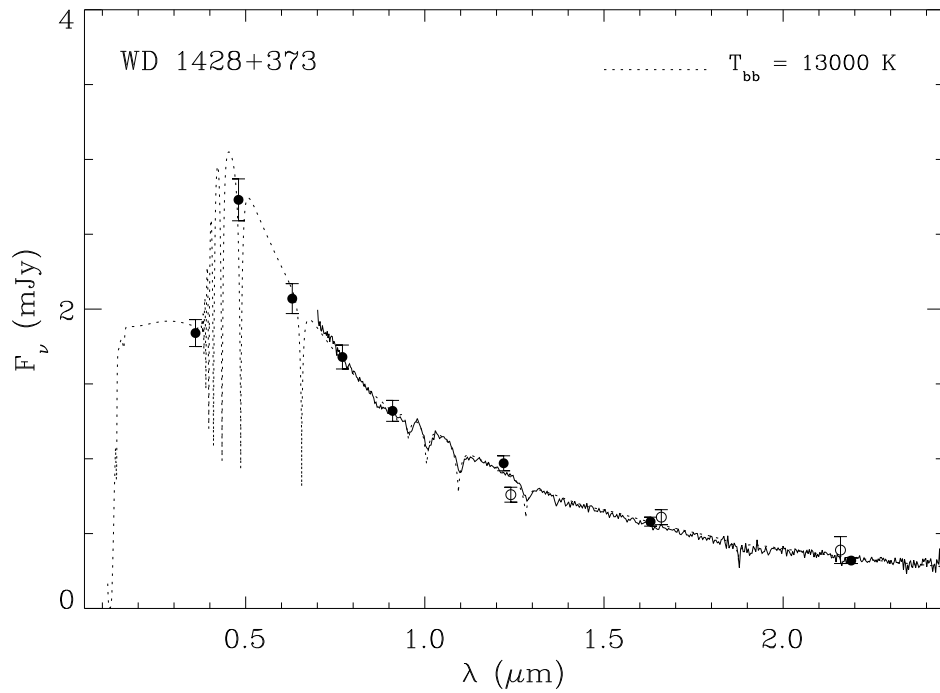


Figure A32. Spectral energy distribution of PG 1428+373. The solid circles are SDSS *ugriz*, and IRTF *JHK* photometry, while the open circles are 2MASS *JHK_s* photometry. The 0.7 – 2.5 μm spectrum was taken with SpeX. There are no *GALEX* data available for this star, and there is no photometric evidence of the known white dwarf companion (Morales-Rueda et al. 2005).

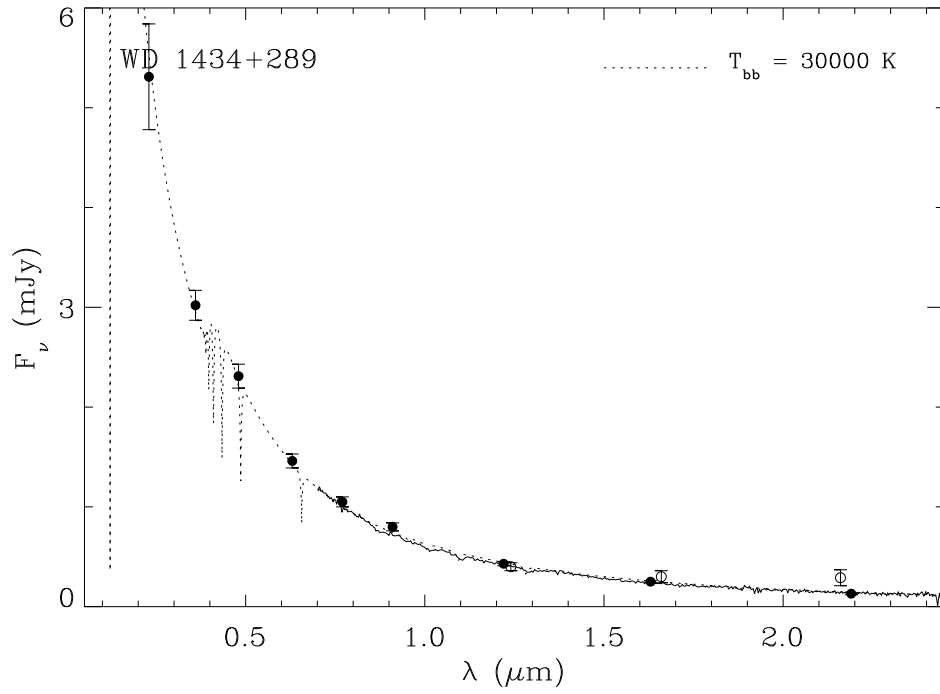


Figure A33. Spectral energy distribution of TON 210. The solid circles are *GALEX* far- and near-ultraviolet, SDSS *ugriz*, and IRTF *JHK* photometry, while the open circles are 2MASS *JHK_s* photometry. The *GALEX* far-ultraviolet flux of 7.8 ± 0.8 mJy is not shown for scaling purposes. The $0.7 - 2.5 \mu\text{m}$ spectrum was taken with SpeX.

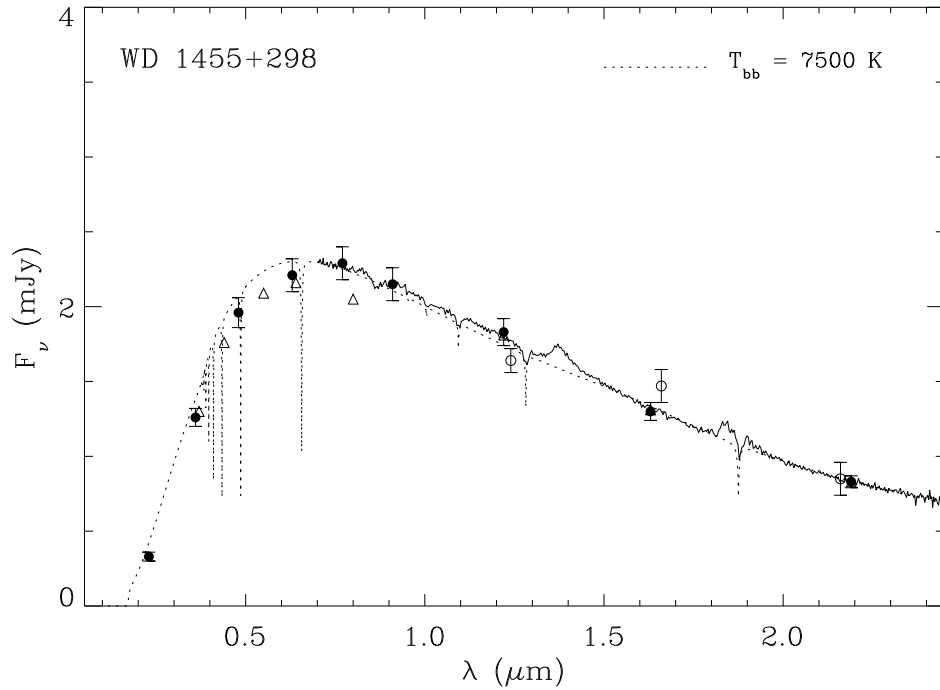


Figure A34. Spectral energy distribution of G166-58. The solid circles are *GALEX* near-ultraviolet, SDSS *ugriz*, and IRTF *JHK* photometry, while the open circles are 2MASS *JHK_s* photometry. The open triangles are *UBVRJHK* photometry from Bergeron et al. (2001); McCook & Sion (1999), and the $0.7 - 2.5 \mu\text{m}$ spectrum was taken with SpeX, which suffers from poor telluric correction.

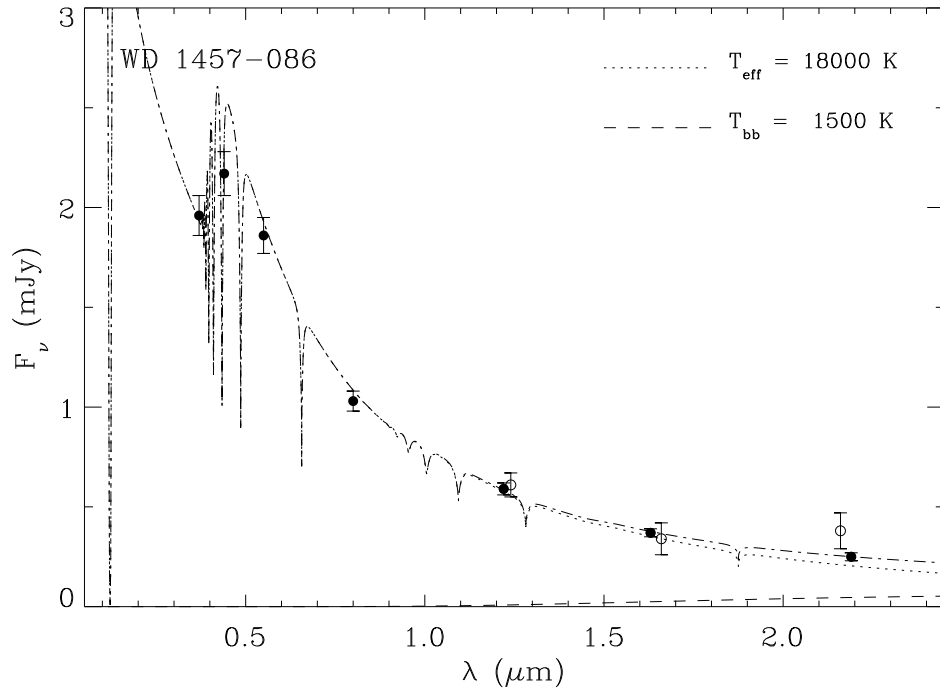


Figure A35. Spectral energy distribution of PG 1457–086. The solid circles are optical *UBVI* and IRTF *JHK* photometry, while the open circles are 2MASS *JHK_s* photometry. There are no *GALEX* data available for this star.

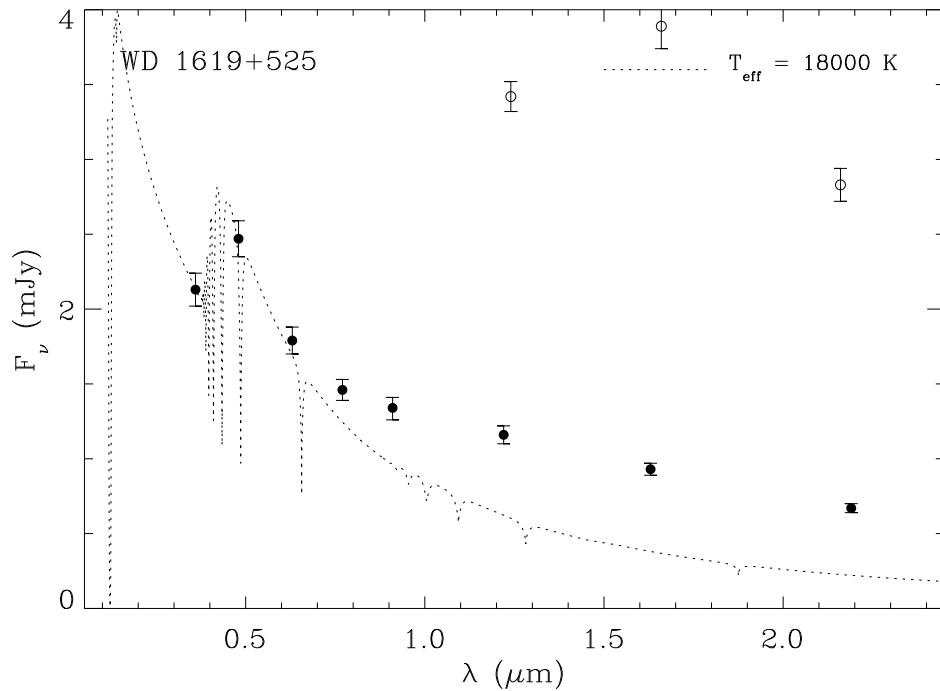


Figure A36. Spectral energy distribution of PG 1619+525AB. The solid circles are SDSS *ugriz*, and IRTF *JHK* photometry. The open circles are 2MASS *JHK_s* fluxes, primarily due to the light of PG 1619+525C, which does not contaminate the IRTF photometry. The secondary star is spatially resolved only in *HST* / *ACS* observations (Farihi et al. 2006). There are no *GALEX* data available for this star.

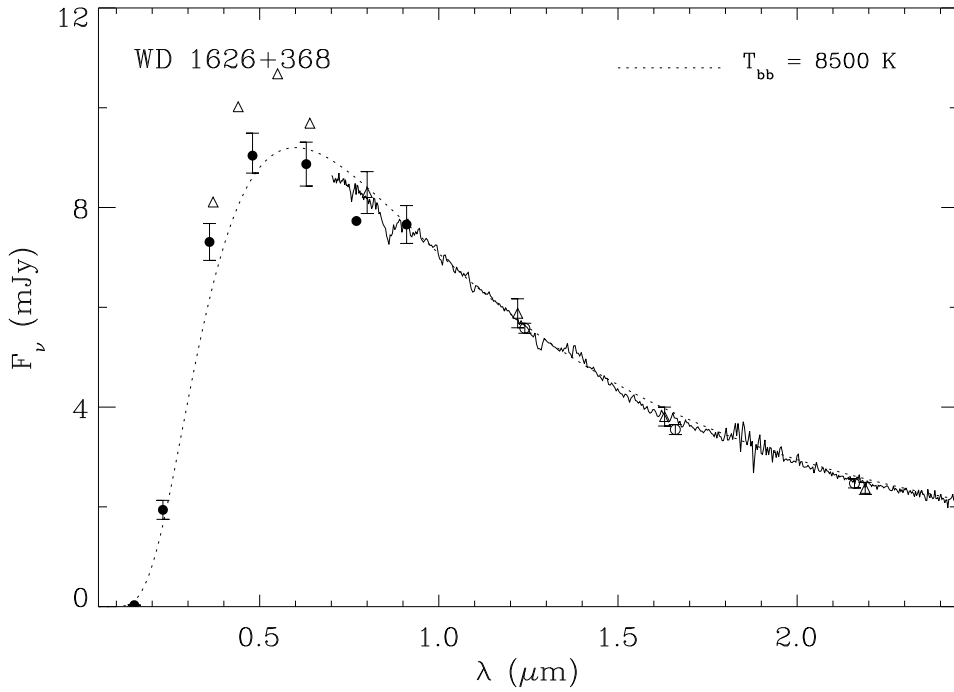


Figure A37. Spectral energy distribution of G180-57. The solid circles are *GALEX* far- and near-ultraviolet, SDSS *ugriz*, and IRTF *JHK* photometry, while the open circles are 2MASS *JHK_s* photometry. The open triangles are *UBVR IJHK* photometry from Bergeron et al. (2001); McCook & Sion (1999), and the 0.7 – 2.5 μm spectrum was taken with SpeX; the calcium absorption triplet centered near 8600 Å is clearly detected.

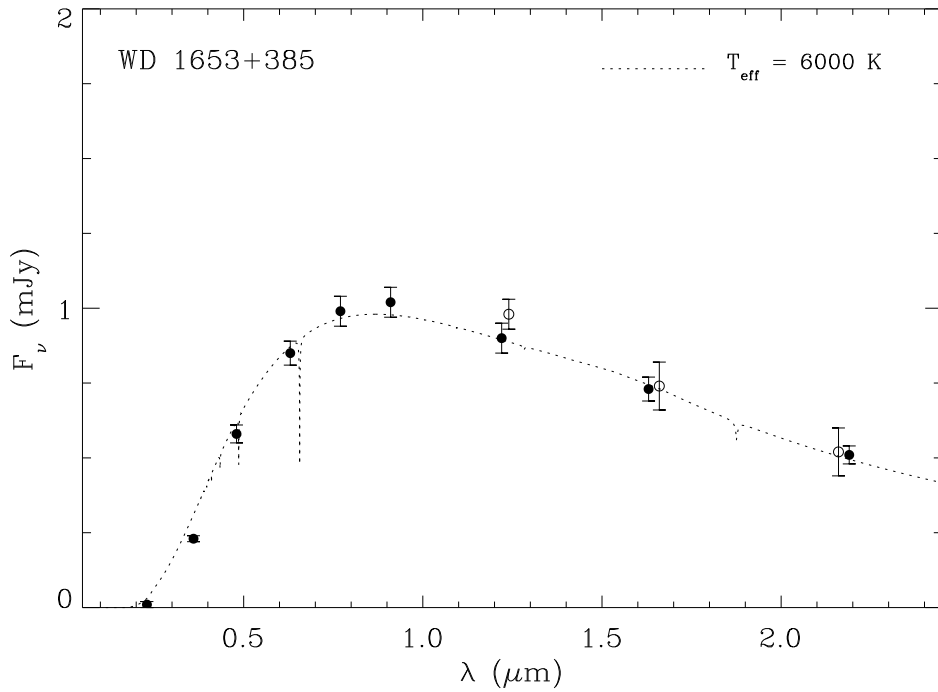


Figure A38. Spectral energy distribution of NLTT 43806. The solid circles are *GALEX* near-ultraviolet, SDSS *ugriz*, and IRTF *JHK* photometry, while the open circles are 2MASS *JHK_s* photometry.

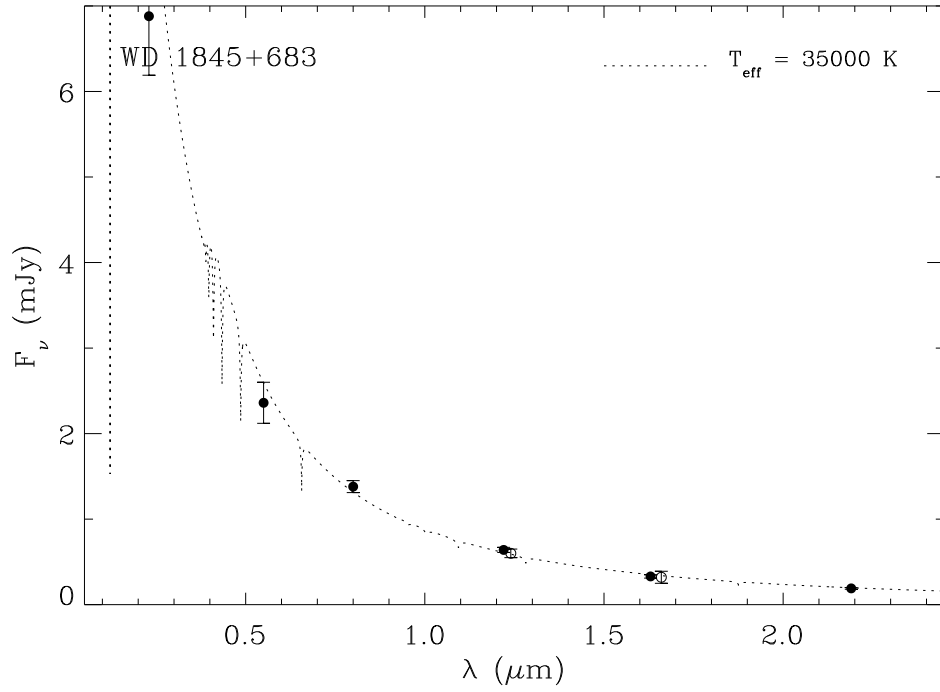


Figure A39. Spectral energy distribution of KUV 1845+683. The solid circles are *GALEX* near-ultraviolet, optical *VI*, and IRTF *JHK* photometry, while the open circles are 2MASS *JHK_s* photometry. The *GALEX* far-ultraviolet flux of 14.1 ± 0.7 mJy is not shown for scaling purposes.

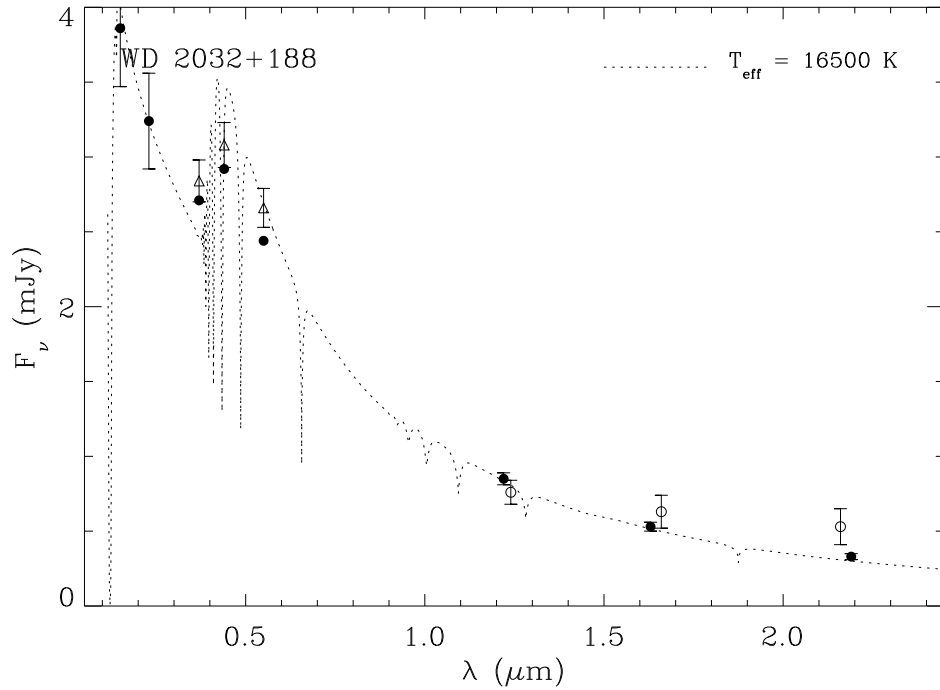


Figure A40. Spectral energy distribution of GD 231. The solid circles are *GALEX* far- and near-ultraviolet, optical *UBV* (average values from McCook & Sion 1999), and IRTF *JHK* photometry, while the open circles are 2MASS *JHK_s* photometry. The open triangles are *UBV* from Eggen (1968).

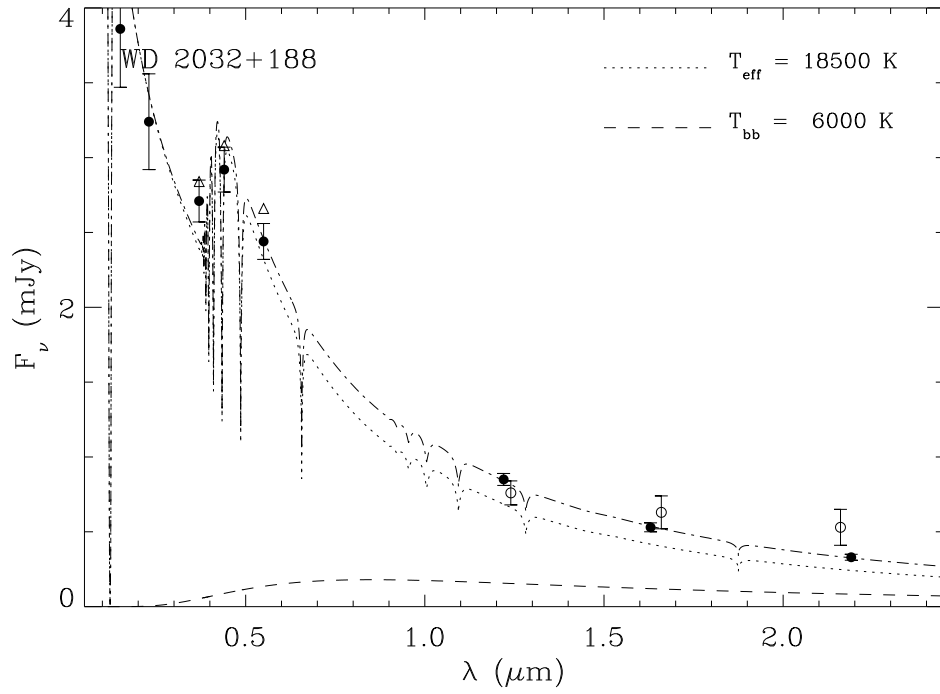


Figure A41. Same as Figure A40 but fitted with the effective temperature of Bergeron et al. (1992). In this case the near-infrared data reveal a mild photometric excess consistent with a cool white dwarf companion.

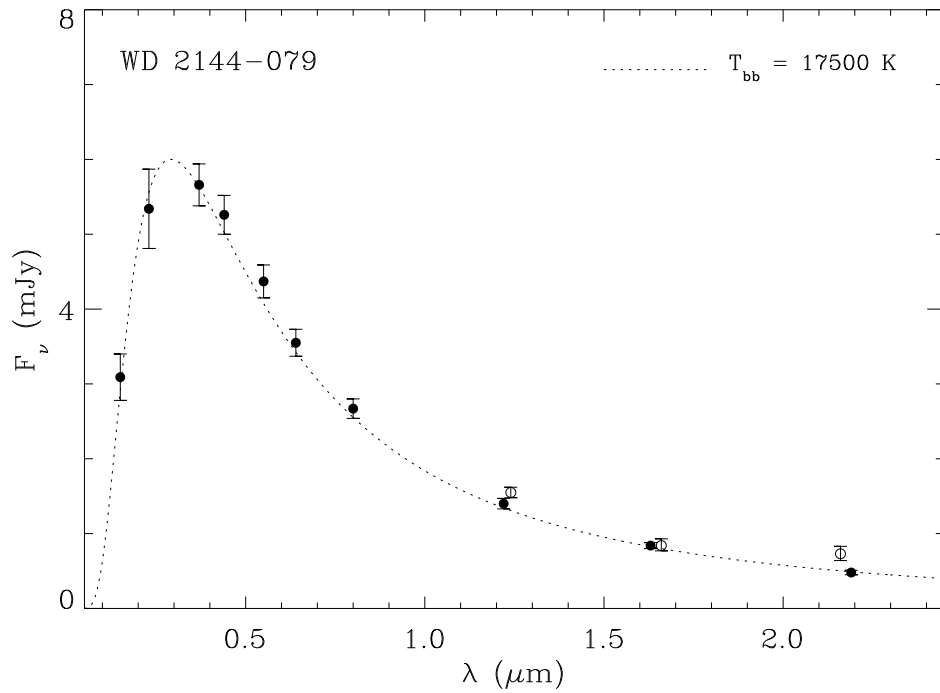


Figure A42. Spectral energy distribution of G26-31. The solid circles are *GALEX* far- and near-ultraviolet, optical *UBVRI*, and IRTF *JHK* photometry, while the open circles are 2MASS *JHK_s* photometry.

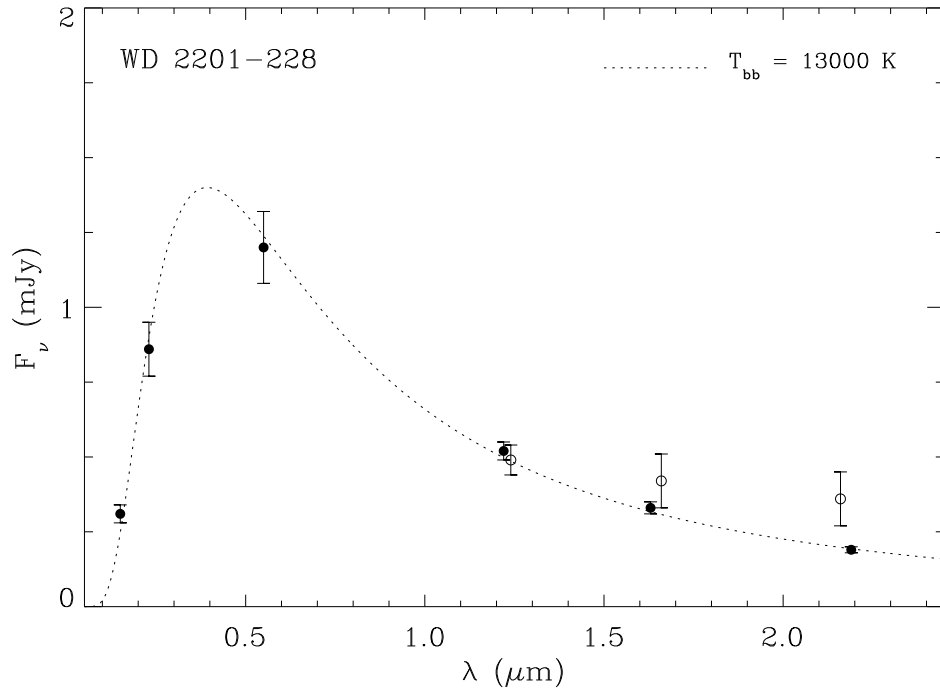


Figure A43. Spectral energy distribution of HE 2201–228. The solid circles are *GALEX* far- and near-ultraviolet, estimated optical *V*, and IRTF *JHK* photometry, while the open circles are 2MASS *JHK_s* photometry.

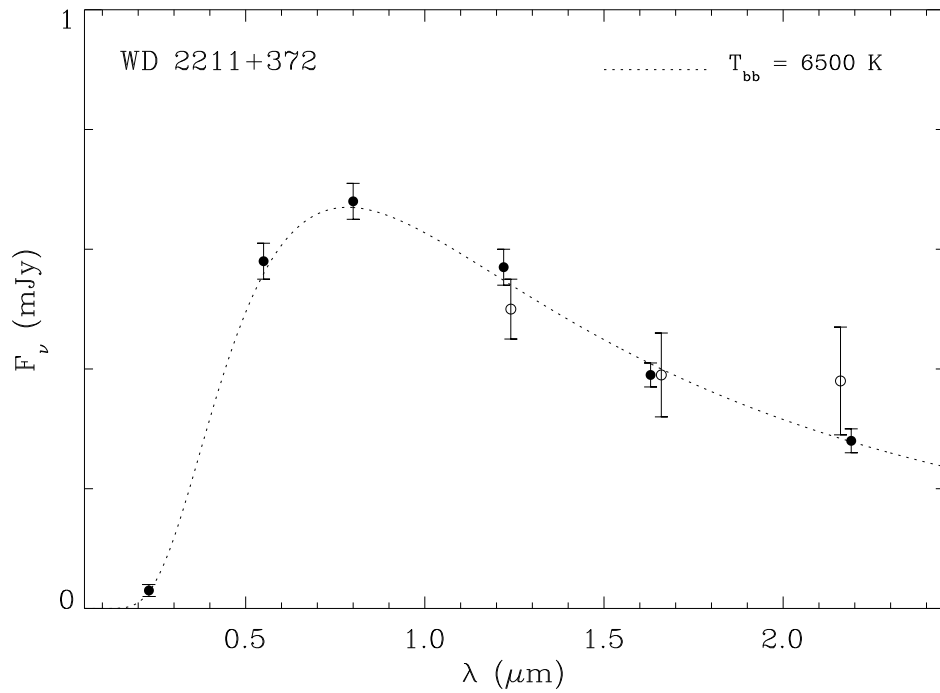


Figure A44. Spectral energy distribution of LHS 3779. The solid circles are *GALEX* near-ultraviolet, optical *VI*, and IRTF *JHK* photometry, while the open circles are 2MASS *JHK_s* photometry.

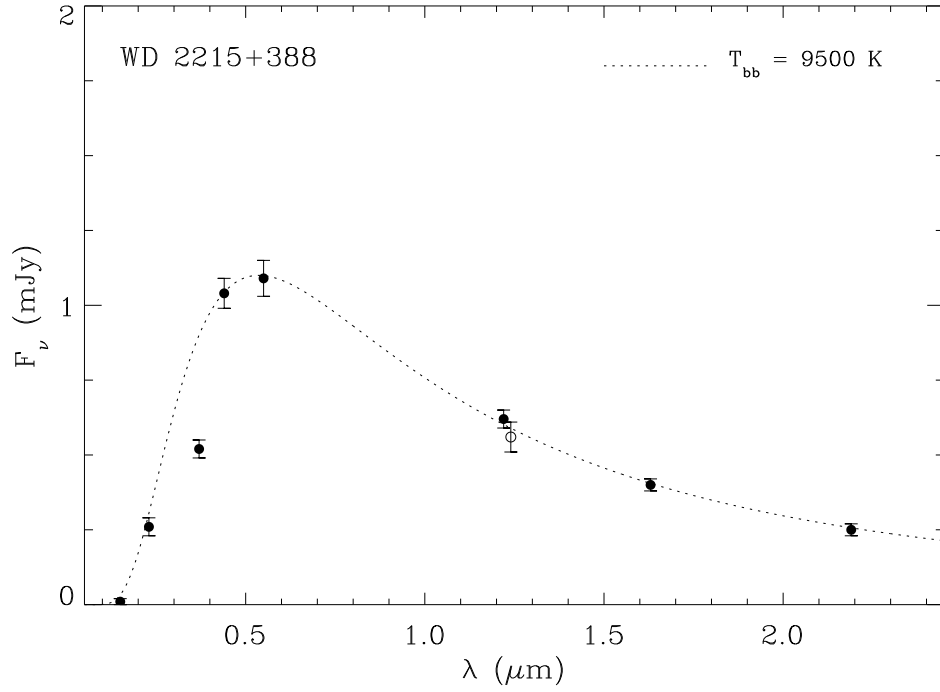


Figure A45. Spectral energy distribution of GD 401. The solid circles are *GALEX* far- and near-ultraviolet, optical *UBV*, and IRTF *JHK* photometry, while the open circles are 2MASS *JHK_s* photometry. This star has very strong Ca H and K absorption (Sion et al. 1990).

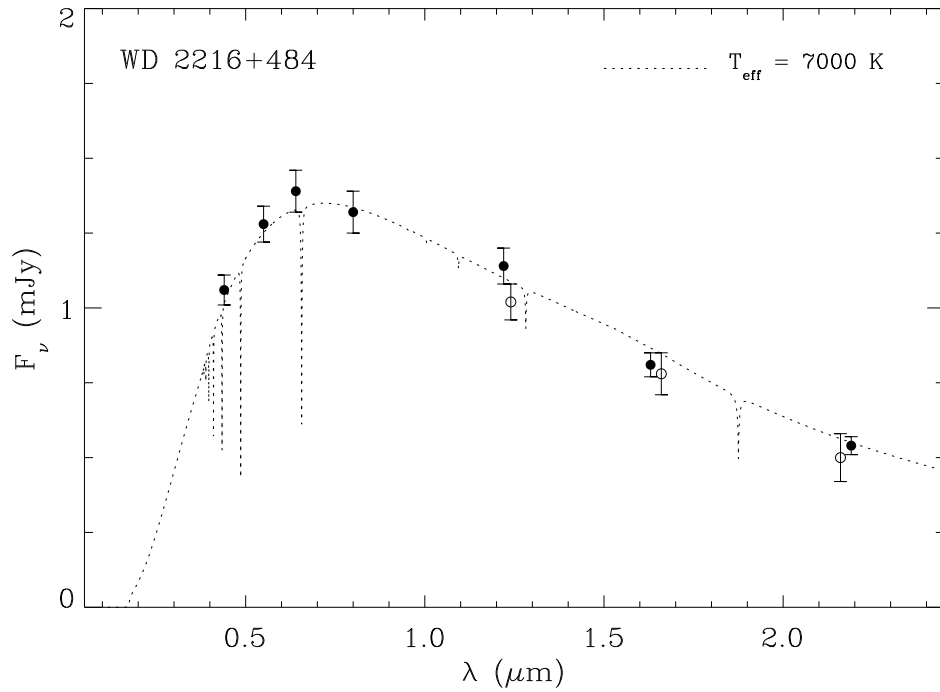


Figure A46. Spectral energy distribution of GD 402. The solid circles are optical *BVRI*, and IRTF *JHK* photometry, while the open circles are 2MASS *JHK_s* photometry. It is possible the full spectral energy distribution is better reproduced by two components (Bergeron et al. 1990). There are no *GALEX* data available for this star.

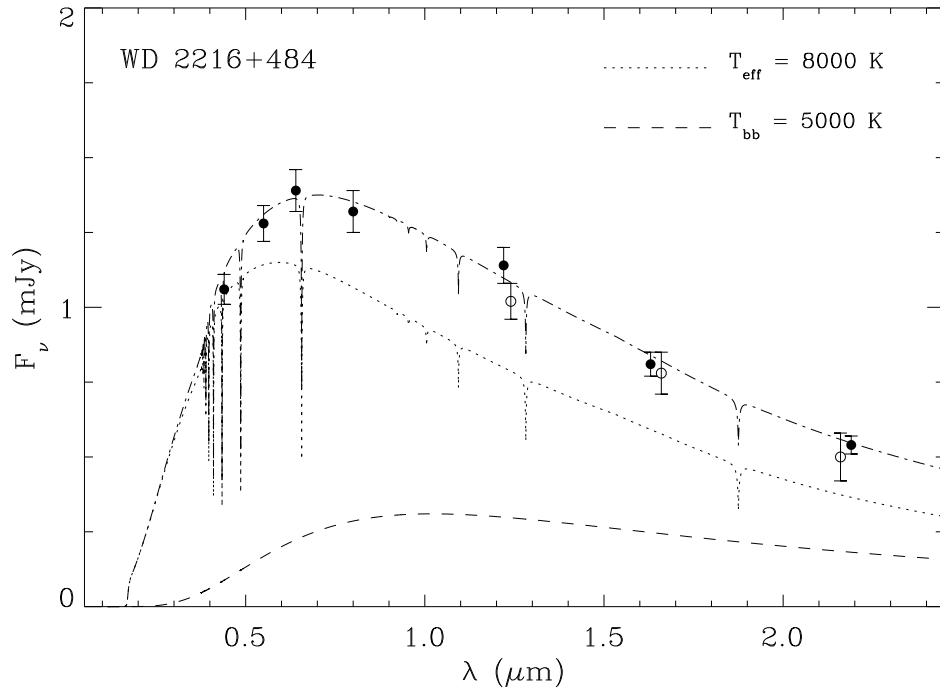


Figure A47. Same as Figure A46 but now fitted with two white dwarf components, similar to the suggestion of Bergeron et al. (1990).

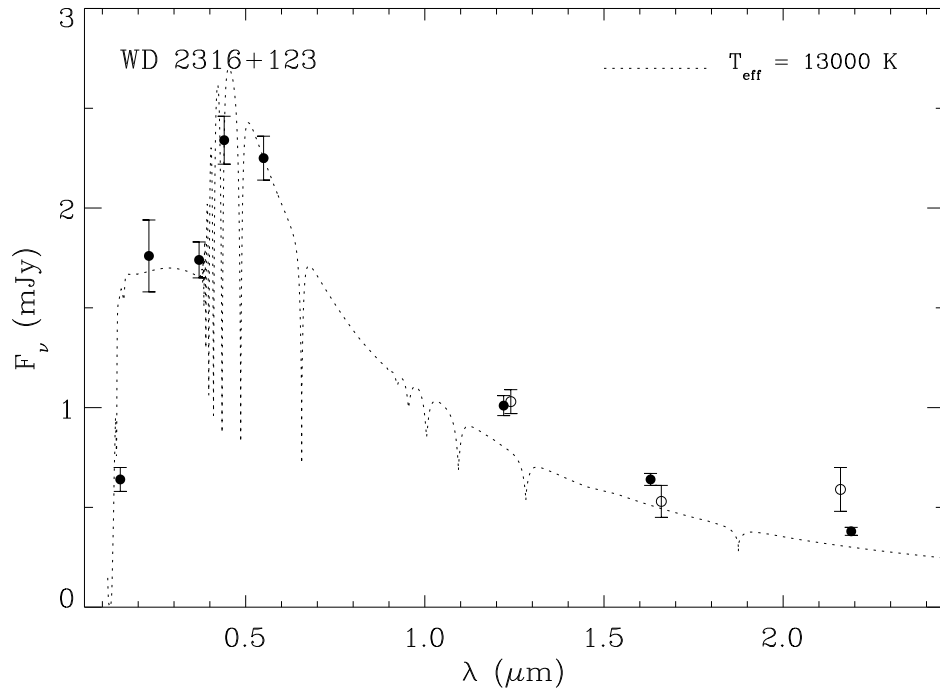


Figure A48. Spectral energy distribution of KUV 2316+123. The solid circles are *GALEX* far- and near-ultraviolet, optical *UBV*, and IRTF *JHK* photometry, while the open circles are 2MASS *JHK_s* photometry. The spectral energy distribution is not reproduced by a single stellar effective temperature, non-magnetic DA model.

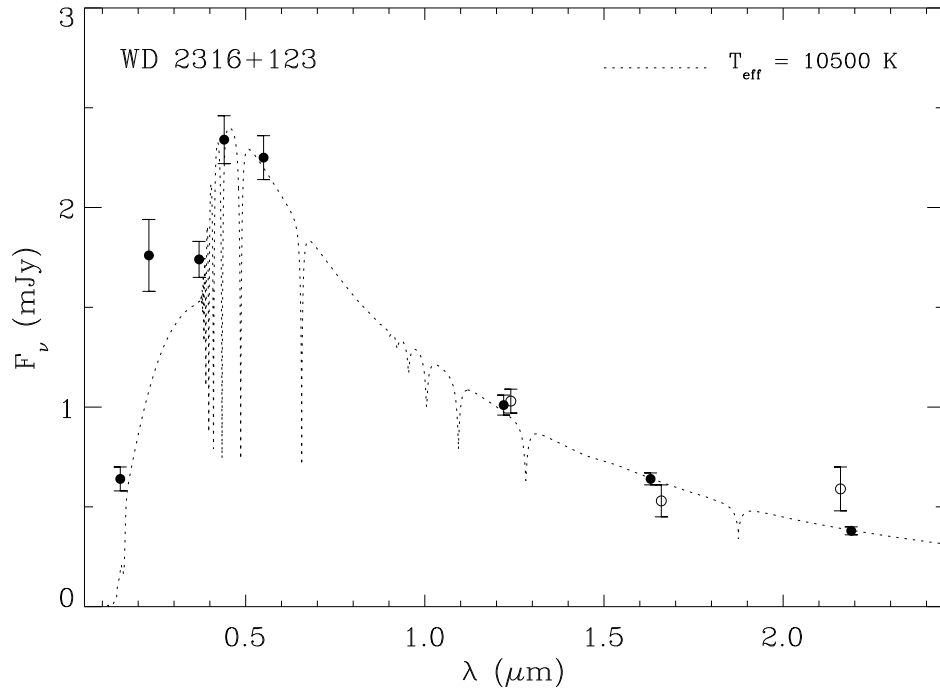


Figure A49. Same as Figure A48 but now fitted with the effective temperature estimate of Liebert et al. (1985); this model underpredicts the ultraviolet fluxes.

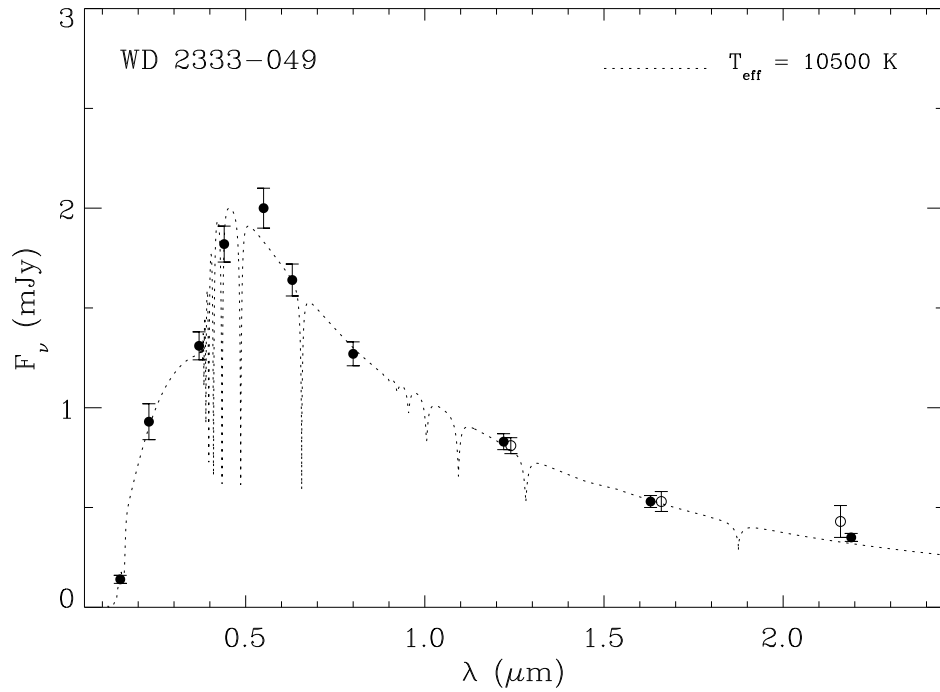


Figure A50. Spectral energy distribution of G157-82. The solid circles are *GALEX* far- and near-ultraviolet, optical *UBVrI*, and IRTF *JHK* photometry, while the open circles are 2MASS *JHK_s* photometry. This star may have a slight *K*-band excess.

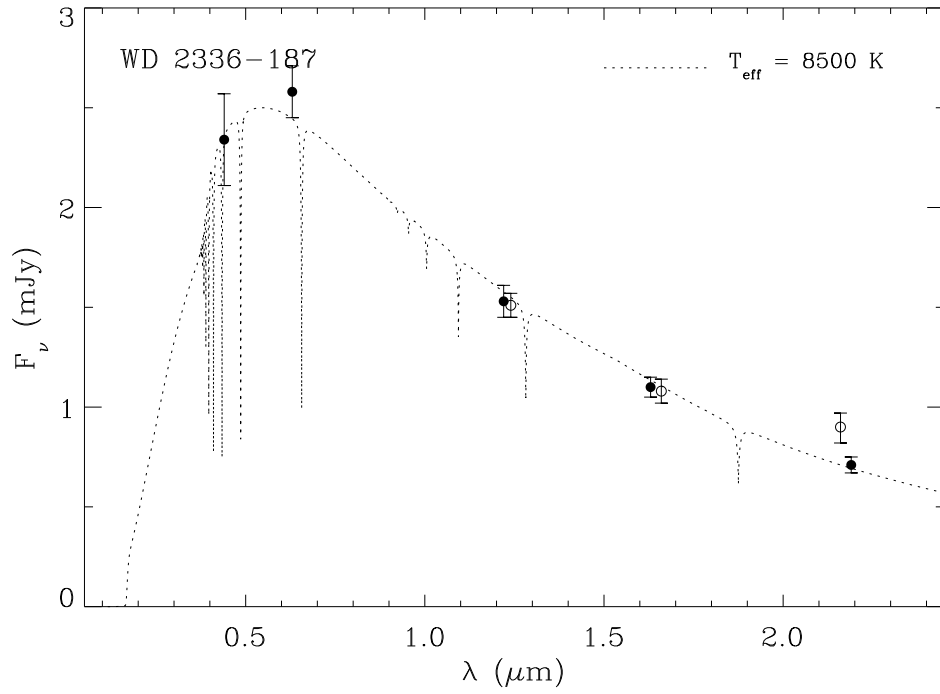


Figure A51. Spectral energy distribution of G273-97. The solid circles are *GALEX* far- and near-ultraviolet, optical *Br*, and IRTF *JHK* photometry, while the open circles are 2MASS *JHK_s* photometry.

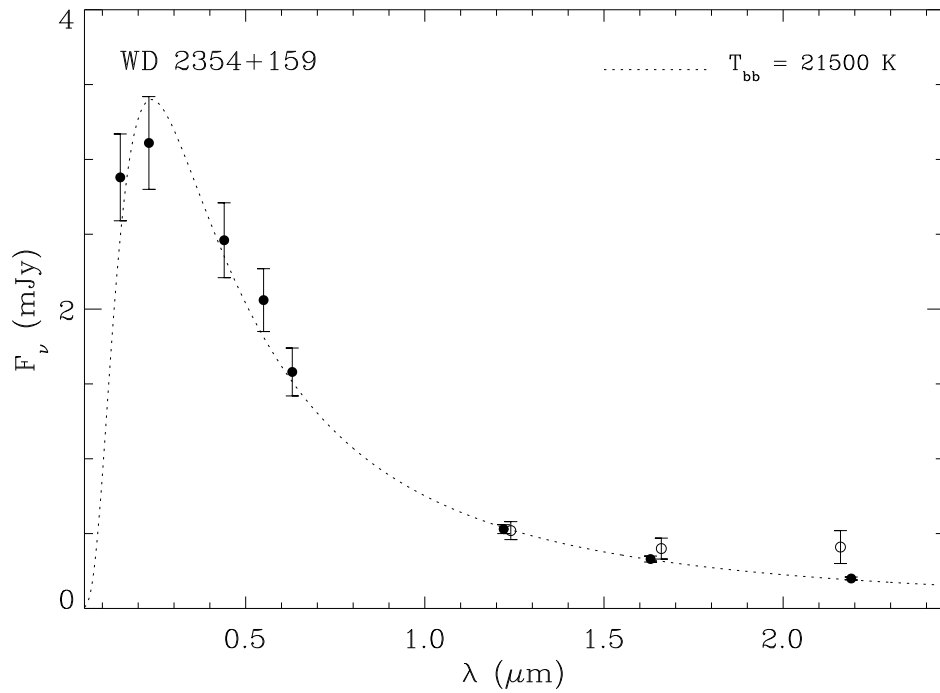


Figure A52. Spectral energy distribution of PG 2354+159. The solid circles are *GALEX* far- and near-ultraviolet, optical *BVR*, and IRTF *JHK* photometry, while the open circles are 2MASS *JHK_s* photometry.